AD-A186 195 IONIC MECHANISMS OF SOOT FORMATION IN FLAMES(U) 1/1
AEROCHEM RESEARCH LABS INC PRINCETON NJ
H F CALCOTE ET AL JUN 87 AFOSR-TR-87-1197
UNCLASSIFIED F49620-83-C-0150 F/G 21/2 NL

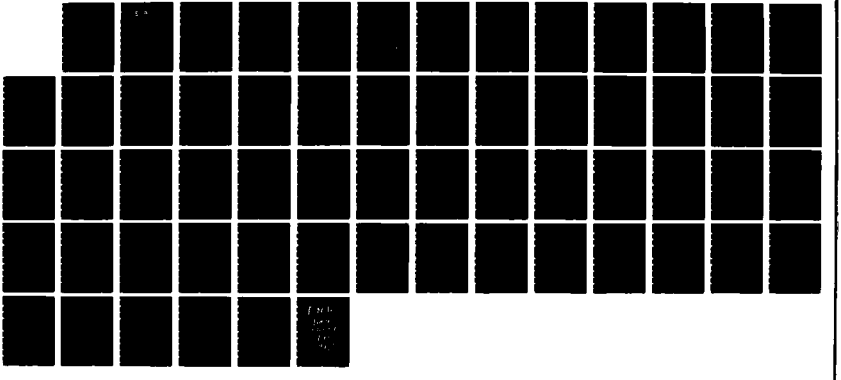

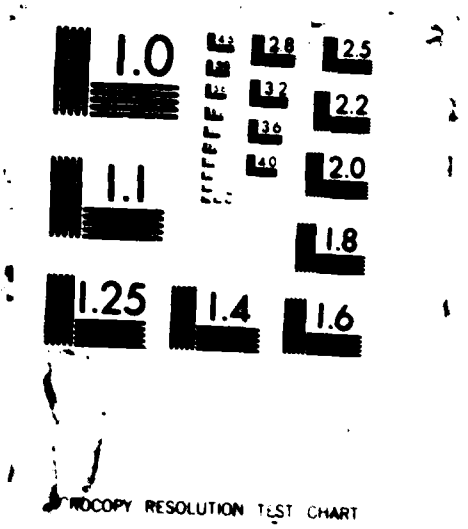
1.0
2.8
2.5
3.2
2.2
3.6
4.0
1.1
2.0
1.8
1.25
1.4
1.6
ROCOPY RESOLUTION TEST CHART

AD-A186 195

2

REPORT DOCUMENTATION PAGE

1a. REPORT SECURITY CLASSIFICATION: Unclassified	1b. RESTRICTIVE MARKINGS: None
2a. SECURITY CLASSIFICATION AUTHORITY:	3. DISTRIBUTION/AVAILABILITY OF REPORT: Distribution unlimited; approved for public release
2b. DECLASSIFICATION/DOWNGRADING SCHEDULE:	
4. PERFORMING ORGANIZATION REPORT NUMBER(S): D	5. MONITORING ORGANIZATION REPORT NUMBER(S): AFOSR-TR. 87-1197
6a. NAME OF PERFORMING ORGANIZATION: AeroChem Research Labs., Inc.	6b. OFFICE SYMBOL (If applicable):
6c. ADDRESS (City, State and ZIP Code): P.O. Box 12, Princeton, NJ 08542	7a. NAME OF MONITORING ORGANIZATION: Air Force Office of Scientific Research
	7b. ADDRESS (City, State and ZIP Code): BA 410 Bolling AFB DC 20332-6448
8a. NAME OF FUNDING/SPONSORING ORGANIZATION: Air Force Office of Sci. Res.	8b. OFFICE SYMBOL (If applicable): AFOSR/NA
8c. ADDRESS (City, State and ZIP Code): Bolling AFB DC 20332-6448 BC 141 C	9. PROCUREMENT INSTRUMENT IDENTIFICATION NUMBER: F49620-83-C-0150
	10. SOURCE OF FUNDING NOS.

PROGRAM ELEMENT NO.	PROJECT NO.	TASK NO.	WORK UNIT NO.
61102F	2308	A2	

11. TITLE (Include Security Classification): Ionic Mechanisms of Soot Formation in Flames

12. PERSONAL AUTHOR(S): H.F. Calcote and D.G. Keil

13a. TYPE OF REPORT	13b. TIME COVERED	14. DATE OF REPORT (Yr., Mo., Day)	15. PAGE COUNT
Final	FROM 9/15/83 TO 9/31/86	June 1987	58

16. SUPPLEMENTARY NOTATION

17. COSATI CODES		
FIELD	GROUP	SUB GR.
21	01	
21	02	

18. SUBJECT TERMS (Continue on reverse if necessary and identify by block number): Soot Formation; Ionic Mechanisms; Flame Measurements; Mass Spectrometry; Langmuir Probes; Thermocouple Probes;

19. ABSTRACT (Continue on reverse if necessary and identify by block number)

Experimental measurements have been made and interpreted in acetylene/oxygen and benzene/oxygen/argon flames at 2.7 kPa, and an unburned flow velocity of 50 cm/s with the objective of evaluating the ionic mechanism of soot nucleation. This mechanism postulates that chemi-ions are the precursors of soot and that the initial reactions in the soot nucleation process are ion-molecule reactions in which molecular ions continually increase in size until they are neutralized by ion recombination. Total ion profiles were determined by Langmuir probe; individual ion profiles were determined by molecular ion sampling mass spectrometry up to about mass 600; temperature profiles were determined by radiation corrected thermocouples It is demonstrated that the ion concentration peaks ahead of the appearance of soot; the ion concentration is greater than the concentration of soot particles; and ions decay as soot is produced. In the acetylene/oxygen $\phi = 3$ flame, the ion-molecule reaction rates are measured and compared with other

(over)

20. DISTRIBUTION/AVAILABILITY OF ABSTRACT	21. ABSTRACT SECURITY CLASSIFICATION
UNCLASSIFIED/UNLIMITED ☒ SAME AS RPT. ☐ DTIC USERS ☐	Unclassified

22a. NAME OF RESPONSIBLE INDIVIDUAL	22b. TELEPHONE NUMBER (Include Area Code)	22c. OFFICE SYMBOL
Julian M. Tishkoff	(202) 767-4935	AFOSR/NA

DD FORM 1473, 83 APR EDITION OF 1 JAN 73 IS OBSOLETE.

Unclassified
SECURITY CLASSIFICATION OF THIS PAGE

BLOCK 18 (Continued)

Ion-Molecule Reaction Rates

BLOCK 19 (Continued)

measured and calculated rates. It is demonstrated that these rates are rapid at flame temperatures. Some major differences were found in the features of benzene and acetylene ion profiles that remain to be explained. The experiments are strongly supportive of the ionic mechanism of soot formation in flames.

TP-465

TABLE OF CONTENTS

LIST OF TABLES

LIST OF FIGURES

LIST OF FIGURES (Continued)

I. INTRODUCTION

For a number of years the personnel at AeroChem have been protagonists of the ionic mechanism of soot formation in flames. In this theory, it is assumed that chemi-ions grow very rapidly through a series of ion-molecule reactions to produce large ions which are neutralized to produce either very small incipient soot particles, or very large neutral molecules which rapidly grow to form the incipient soot particles. We have, in fact, previously demonstrated that there is no sharp demarcation between large molecules and small soot particles.[1,2]

After much study by many people, an understanding of the soot nucleation process still represents one of the more significant problems challenging the combustion community. Much of the reason for this is that the necessary data required to resolve the many questions about the initial stages of soot formation--where the major questions apply--are very difficult to obtain experimentally; global measurements of soot particles do not give the necessary information. The objective of our program has been to make the necessary detailed ion (both total and individual) concentration profile measurements in the same flames in which Howard and associates at MIT[3-6] and others, e.g., Delfau and associates[7-9] in France, and Homann and associates in Germany[10-13] are making complementary measurements. Our measurements included: mass spectrometer measurements for individual ion concentrations; Langmuir probe measurements for total ion concentrations; and temperature compensated thermocouple measurements for temperature profiles. To assure that the flames we study are exactly comparable to those used by Howard and associates at MIT, we have duplicated their burner.

The work statement for this program contained two phases. Phase I experiments were to be done in well studied flames of benzene-oxygen and acetylene-oxygen and they included generation of temperature profiles, Langmuir probe curves of total ion concentration, and mass spectrometer profiles of individual ions. Phase II involved model development of the individual processes involved in incipient soot formation, e.g., rates of ion and particle formation, rates of production of large molecular ions, the temperature of the growing particle and its effect on thermal ionization, thermal ionization of large molecules, and ion molecule rate coefficients. The quantitative models developed in this program for each of the steps will form the basis for a detailed overall quantitative model of the total process of soot formation. Considerably more time was consumed in the calibration of the mass scale of the mass spectrometer than anticipated but this was necessary in order to treat the problem quantitatively. This was done at the expense of other experimental tasks.

In this report we summarize the results on this program. Results which have been published are only briefly summarized; other results are covered in more detail.

II. APPARATUS AND EXPERIMENTAL TECHNIQUES

A. APPARATUS

The apparatus used in the mass spectrometric studies consists of a multi-tubular burner supported on a vertical translation stage which feeds through a vacuum seal into a cylindrical flame chamber pumped by a large (140 L s^{-1}) mechanical pump. The top of the chamber is fitted with a water-cooled plate supporting a metal sampling cone which permits the sampling of flame gases through an (0.013-0.025 cm) orifice into the first of two differentially pumped vacuum chambers. This chamber, maintained at less than 0.01 Pa pressure, contains a series of electrostatic lenses which focus and direct the flame ion beam into the second vacuum chamber containing a quadrupole mass filter, maintained at pressures below 0.001 Pa by a 15 cm (6 in.) diffusion pump. The quadrupole used in this work was constructed at AeroChem about 20 years ago. In this study it was powered by a 350 kHz rf supply providing a useful mass range up to nearly 600 amu. Ions which pass through the mass filter strike the cathode of an electron multiplier and the amplified current is recorded on an XY recorder as a function of mass (fixed burner position) or as a function of burner position (fixed ion mass). A digitizer pad was used to transfer mass spectrometer data from recorder charts to a computer for processing.

B. MIT BURNER

The copper burner used by Bittner and Howard[5] at MIT was duplicated from designs furnished by Howard[14] so we could compare our ion profiles with their profiles of neutral species in the same flames. It consists of three major pieces. The burner surface is a 7.1 cm diameter, 1.27 cm thick copper plate with about 600 1 mm holes drilled in a hexagonal close-packed pattern such that the center to center distance is 0.254 cm. This plate is press-fit into a thin-walled (0.3 cm thick) support cylinder, which is threaded onto the bottom mixing chamber and water-cooling chamber. Therefore the burner surface is cooled by conduction down the copper support cylinder to the water jacket at the burner base. This burner operates with a surface temperature ($\approx$ 425 $\pm$ 25 K at burner edge) which is greater than our directly cooled stainless steel burner.[15] We had considerable difficulties getting this burner to operate in our system; the flame showed a slow periodic oscillation. We finally traced this problem to a gas mixing chamber and eliminated the difficulty by simply changing the manner in which the two gases were brought into the chamber. No similar problem was observed with our stainless steel burners which have larger pressure drops across the burner.

C. TEMPERATURE MEASUREMENTS

Accurate temperatures are required to interpret the various data to be analyzed and they are generally not available in the flames in which we were

interested. Measurement of flame temperatures in sooting flames is a complicated problem and is thus often avoided or done without correcting for radiation losses. We thus report our procedures here in some detail; we plan to publish this work in the future.

For our primary measurements we chose to use a thermocouple technique in which radiation losses are compensated for by electrical heating of the thermocouple,[16] but because of this technique's complexity, we also used it to calibrate the radiation corrections of coated thermocouples which were not electrically heated. As a check, these radiation corrections were also calculated by the usual techniques. Fine wire S-type and B-type thermocouples 1 to 2 cm long with diameters from 50 to 125 μm were fused onto 250 μm wires of the same materials as saddle supports. The support wires fed through an alumina tube which was in turn inserted into a stainless steel 0.64 cm o.d. tube, vacuum-sealed with epoxy cement, and brought through the low pressure burner housing wall through a sliding O-ring seal.

In nonsooting flames catalytic heating of the thermocouple was avoided by coating the thermocouple with BeO/Y_2O_3.[17] The coating was fused at about 1870 K in a Meeker flame. In sooting flames the soot which rapidly formed on the probe was found to be a good noncatalytic coating. In some cases the thermocouple was intentionally soot-coated in a rich flame and rapidly used in a nonsooting flame before the coating burned off. The diameters of coated wires were measured before and after the experiments using a microscope to determine the coating thickness which was typically about 10-15 μm.

In the electrically heated thermocouple method, the thermocouple temperature is measured in a vacuum ($\leq 3 \times 10^{-3}$ Pa) as a function of heating current. This is done by resistively heating the wire with a 3 kHz a.c. current and simultaneously measuring the d.c. thermal emf of the thermocouple junction. In a good vacuum the convection losses are small or negligible so that the electrical power loss in the wire is equal to the radiation losses. A plot of junction temperature vs. heating current is thus generated. The experiment is then repeated in the flame producing another (different) plot of thermocouple temperature vs. heating current. If the two curves (one obtained in vacuum and one in the flame) are plotted on the same coordinate system they will cross at some point. If the radiative properties of the thermocouple (ϵ and d_w, where ϵ = the wire emissivity and d_w = the thermocouple wire diameter) do not change between the two experiments, the temperature at the crossing point is the true flame temperature. At this point there are no net losses from the thermocouple. To assure that the radiation properties of the thermocouple do not change during each experiment, the temperature-current curve is repeated in vacuum after each flame experiment.

The above procedure is tedious, and due to the fragile nature of the wire coating it was necessary to produce heating curves rapidly before the surface properties changed. Many thermocouples were lost, especially at the highest temperatures so that extrapolation procedures were developed.

Under vacuum conditions, in the absence of convection and conduction losses at the thermocouple junction, the energy balance involves only electrical heating and radiative losses to the surroundings. Equating the rates per unit wire length:

$$\sigma \epsilon \pi d_T \ (T_w^4 - T_s^4) = \frac{4\rho}{\pi d_w^2} \ I^2$$

where σ is the Stefan-Boltzmann constant, d_T is the total wire plus coating diameter, d_w is the diameter of the wire itself, ρ is the resistivity of the junction area and I is the heating current. The wire temperature, T_w, is much greater than the temperature of the surroundings, T_s so that

$$\sigma \epsilon \pi d_T \ T_w^4 = \frac{4\rho}{\pi d_w^2} \ I^2$$

The current required to heat the thermocouple to a temperature T_w is then:

$$I \propto d_w \left(\frac{d_T \epsilon}{\rho} \right)^{0.5} T_w^2$$

For platinum and rhodium alloys, both ϵ and ρ show similar temperature dependencies in the range of interest, 1000-2000 K. Therefore the overall current to temperature proportionality is $I \propto T_w^2$.

The calculated slopes dI/dT^2 should provide a measure of $(\epsilon d_T)^{0.5}$. The experimental values were grouped by the thermocouple visual appearance and dI/dT^2 normalized (to a new, shiny thermocouple). Slopes are given here:

Appearance	$(dI/dT_w^2)/(dI/dT_w^2)_{new, shiny}$
Bare, shiny	1.00
Bare, not shiny	1.43
Bare, rough	1.57 ± 0.08
Dark coating, smooth - same diameter	1.80 ± 0.10
Dark coating, rough - same diameter	1.86 ± 0.05
Clean BeO/Y_2O_3 - thick	1.96
Dark BeO/Y_2O_3 - thick	2.36

This provides a rationale for extrapolation of the vacuum heating curves. Over 20 heating curves in vacuum were made for variously treated thermocouples. The current required to heat the thermocouples to any fixed temperature varied by nearly a factor of three, yet a linear least squares fit of T_w^2 vs. I, always gave a correlation coefficient $r^2 > 0.99$. The T_w^2 vs. I fitting routine was thus used to extrapolate to temperatures not directly accessible. The heating curves in the flame environment do not lend themselves to such

simple closed form analysis since the convective heat transfer to the wire has a different temperature dependence from the radiation.

Three sets of heating curves are shown in Fig. 1 for two different thermocouples (circles and triangles) in a $\emptyset = 2.25$ flame, 21 mm above the burner and for one thermocouple (squares) 1.5 mm above the burner in the same flame. Thermocouple A was more heavily coated with carbon or soot for these measurements. Both thermocouples were B-type using 51 μm wires. The open symbols represent the vacuum calibration data while the solid symbols represent the heating curves in the flame. The curves through the open symbols are (linear) least squares fits to the data above 1000 K to the form: $I = a + bT_w^2$. (The line through the open circles represents a linear extrapolation of the four data points above 1300 K.) Either extrapolation method gives about the same result at the intersection of the vacuum and flame heating curves. The flame data (solid symbols) exhibit curvature at low currents. However, as the wire temperature increases, the T^4 heat loss term becomes more important and the curvature decreases. Simulated heating curves calculated here have shown that the approach to the flame temperature is well approximated by a linear temperature vs. a.c. current relationship. We feel that a linear extrapolation of the flame data is more realistic, although it is recognized that uncertainties in extended extrapolation can be fairly large. Figure 1 supports the extrapolation method. The two thermocouples used at 21 mm have significantly different heating curves, yet the extrapolated flame temperatures are the same for both cases.

For thermocouples which are not electrically heated ($I = 0$), in the absence of catalytic heating and wire conduction losses (negligible with the long (≈ 1 cm) fine wires used here), the heat balance equation gives the temperature correction for radiation for cylindrical thermocouples,

$$\Delta T \equiv T_{f,i} - T_w \approx \frac{\sigma \epsilon}{h} T_w^4$$

where $T_{f,i}$ is the true local flame temperature, T_w is the thermocouple junction temperature, and h is the heat transfer coefficient from the flame gases to the wire. The temperature of the surroundings to which the thermocouple radiates is assumed to be small relative to T_w. The difference between the flame temperature from the intersection of the heating curves and the thermocouple reading with no heating current is the radiation correction, ΔT. The parameter h can be expressed as

$$h = \frac{k_f \, Nu}{d_f}$$

where k_f is the thermal conductivity of the flame gases and Nu is the Nusselt number. Thus,

$$\Delta T = \frac{\epsilon d_T \sigma T_w^4}{k_f \, Nu}$$

Under conditions appropriate to low Reynolds number, Re, as in these measurements, Nu has been approximated as[18] $0.8(Re)^{0.25}$ and as[19] $(0.42\ Pr^{0.2} + 0.57\ Pr^{0.33}\ Re^{0.5})$ where the Prandtl number Pr is roughly unity. In either case, Nu is only mildly dependent on the thermocouple dimensions ($Re \propto d_T$).

Thus, for the same position in a flame we estimate that the thermocouple response, in terms of $\Delta T/T_w^4$, is proportional to $(d_T \epsilon)$. The vacuum heating curves were shown above to scale as $I \propto (d_T \epsilon)^{0.5} T_w^2$. Therefore the radiation correction should be closely related to the square, $(dI/dT^2)^2$. For the two thermocouples used at 21 mm (Fig. 1) the ratio of the correction term $\Delta T/T_w^4$ is about 0.7 while the ratio of $(dI/dT_w^2)^2$ for the vacuum calibrations is about 0.6, consistent with the predictions.

In addition to the above procedures the heat transfer coefficient was calculated based on Kaskan's treatment[18] which assumes $Nu = 0.8(Re)^{0.25}$. Estimates of the flame composition were obtained from equilibrium calculations. Viscosity was calculated with Wilkes mixture rule and thermal conductivity was calculated with Wissiljewa's mixture rule as described in Ref. 20. For the three calibrations in Fig. 1 the experimental values of ΔT and the calculated values for h were consistent with a reasonable emissivity, $\epsilon = 0.8$. Due to uncertainties in the values of h, we do not claim to have measured ϵ but an elevated emissivity above that for a shiny thermocouple is consistent both with visual observations of carbonaceous coatings formation in these nonsooting flames and with the vacuum calibrations.

Determination of flame temperatures with thermocouple heating curves is both time consuming and tedious. However, one can make use of any single measurement to determine ϵ/h for a thermocouple in a particular flame as described above. Since

$$\frac{\epsilon}{h} = \frac{\epsilon d_T}{k_f \, Nu}$$

one can estimate the variation in ϵ/h and thence the radiation correction, ΔT. The Nusselt number is assumed to only weakly depend on the local flame properties. For a given thermocouple with a fixed surface, ϵd_T is constant. Note that dI/dT_w^2 is a measure of this for any specific thermocouple and can be used to check the thermocouple properties. The thermal conductivity k_f is composition and temperature dependent. However, the major product gases in $\phi = 2.5$ to 3.5 flames have similar thermal conductivities, so the calculated temperature dependence of k_f of about T^1 is the major correction factor. Electrically heated thermocouple temperature measurements were made near the location of the maximum temperature, at T_{MAX}, in the $\phi = 3.0$ flame (at 1.0 cm from burner). The values of 1883 and 1923 K were determined with two different thermocouples. The differences between the uncorrected thermocouple reading in the flame and the flame temperature was on the order of 270-300 K. Two

values of ϵ/h were then calculated and the mean value was used to correct all the flame profiles for $2.5 \leq \phi \leq 3.5$, correcting for the temperature dependence of k_r scaled as T^1. With correction factors on the order of 200 to 400 K, the inclusion of temperature dependent k_r normally changed the correction by less than 40 K. The effect of flame composition variations was assumed to be negligible although this is not a good approximation in the region between the burner and the temperature maximum. However, in this region corrections tend to be lower and limited spatial resolution introduces comparable uncertainties. For example, at 4 mm in a $\phi = 3.0$ flame, the temperature gradient is about 100 K/mm and the estimated thermocouple correction factor is 200 K. A 50% change in the thermal conductivity would cause an error in the corrected temperature only to the spatial resolution of the thermocouple. Because the calculated ion concentrations derived from Langmuir probe data are not greatly affected by errors of this magnitude, we do not attempt more complicated corrections close to the burner.

Measurements were also made in $\phi = 2.25$ flames using the electrical heating technique. As previously shown (Fig. 1) a heavily sooted thermocouple (A) and the lightly sooted thermocouple (B) measurement at 21 mm from the burner gave the same temperature even though radiative properties (vacuum calibrations) differed considerably. The value of ϵ/h extracted for the lightly sooted wire (thermocouple B) was used to correct the temperatures in two rapidly recorded unheated thermocouple profiles as described above. The agreement in the region of overlap was about ± 20 K. Other heating curve measurements of the temperatures nearer the burner, while somewhat uncertain, are in accord with these profiles.

Temperature profiles in leaner flames (e.g., $\phi = 1.5$, 1.75, 2.00) are complicated by catalytic heating. Use of either a heavy BeO/Y_2O_3 coating of 10 to 20 μm thickness or a soot coating (10 μm thickness) eliminated this effect. Both thermocouples had similar dI/dT^2 ($\propto (\epsilon d_T)^{0.5}$) values measured in a vacuum. The assumption of equal values of ϵ/h for the two thermocouples gave about 30-40 K difference between the two experimental temperature profiles in any flame.

Overall, the maximum difference in temperature measured at any point in any flame is about ± 60 K (± 80 K in $\phi = 2.0$) while typically any difference near and downstream of T_{MAX} is closer to ± 30 K (± 40 K in $\phi = 2.0$).

Temperature measurements in several flames of interest were made by the above technique and are reported in Figs. 2 and 3. Figure 2 gives profiles on the AeroChem stainless steel burner at several equivalence ratios, ϕ. The flames are all acetylene-oxygen ($p = 2.7$ kPa, unburned gas velocity $u = 50$ cm/s). In Fig. 3 the temperature profile on the AeroChem stainless steel burner and on the MIT copper burner are compared for a $\phi = 3.0$ flame. In obtaining these data three different thermocouple wire diameters were used, 51, 76, and 127 μm. The range in temperature among them was ≈ ± 2%. The temperature differences between the two burners, Fig. 3, are certainly due to differences in thermal losses, mostly to the cooled burner surface. The calculated adiabatic flame temperature for these conditions is 2772 K. The

temperature profiles decrease with different slopes, e.g., the MIT burner flame temperature decreases more rapidly than does the temperature on the AeroChem stainless steel burner. When the temperature profiles reported here and by others[9,21] are plotted against the distance above the burner divided by the burner diameter, the temperature profiles become parallel, Fig. 4.

D. MASS SPECTROMETER MASS CALIBRATION

Calibration of the mass spectrometer for mass is described in detail in Ref. 22 so will only be summarized here. Metal salts were added to the flame to provide unambiguous mass markers at low masses. The salts of potassium (39 and 41 amu), rubidium (85 and 87 amu), cesium (133 amu), and lead (206 and 208 amu) were used. In order to identify the masses of heavy ions beyond 200 amu, the spectra from fuel rich deuterated acetylene flames were evaluated. Comparison of mass spectra from C_2H_2 and C_2D_2 flames generally showed a one-to-one correspondence for the peaks in the same general pattern of relative intensities; the deuterated ion peaks were shifted to higher mass by a difference that generally increased for larger ions. Each of the ion species exhibited a significant ^{13}C ion peak with intensity, relative to the pure ^{12}C ion, proportional to the number of carbon atoms, e.g., 1.1% per carbon atom.

Mass assignments were made to be consistent with: low mass hydrocarbon ions identified in previous work[7,68] alkali metal and lead ions; and several integer mass relationships, ΔM, between the ions observed in the two isotopic flames. Mass peaks, observed at every carbon number from 3 to 45 (the high mass limit of the instrument), appeared as single peaks in the protonated spectra, but many became multiple peaks upon deuteration.

Our best estimates from the mass calibration for the large ion identities and structures are given in Table I. Alternate structures are possible for some of the ions but given the C/H ratio and the structure rules of organic chemistry there is not as much freedom in choosing a structure as one might initially suppose. Note that the odd carbon number ions can be represented as polycyclic molecular ions while the even carbon number ions are represented as a protonated polycyclic molecule. All of the structures are compact with little branching. (The 2-carbon atom side chains may also appear as condensed 5-member rings in the polycyclic ring system.) The largest ion observed, $C_{45}H_{17}$, mass 557, is still small compared to small soot particles. The molecular ions in Table I would most probably be flat plates with diameters up to about 1.0 nm for mass 557 compared with the 1.5 nm diameter of the smallest observed soot particle.[3]

E. CALIBRATION OF MASS SPECTROMETER SENSITIVITY

Calibrations of the mass spectrometer for sensitivity as a function of mass is described in detail in Ref. 22 so will only be summarized here. One of the major difficulties with mass spectrometer studies of flame ions is that of calibrating the instrument sensitivity, which is mass dependent, to

obtain ion concentrations. A simplified calibration was performed based on our previous Langmuir probe measurements of total ion concentrations in which we have great confidence.[23]

Flame ion spectra, i.e., the currents due to individual ions, were recorded at various distances above the burner. Spectra were also recorded as a function of distance above the burner while operating the mass spectrometer as a high-pass filter (no applied d.c.). In this mode of operation only ions above a fixed mass are sampled. Since there should be less discrimination against high masses in this mode, it provided a better estimate of the relative concentrations of heavy and light ions than using the individual ion currents directly. The integrated currents over a small mass range, in the high-pass filter mode, divided by the sum of resolved ion peak currents over the corresponding mass range was used as a measure of mass discrimination. A calibration function was thus derived and applied to the normalized individual ion current profiles to adjust them to the high-pass filter current values, see Fig. 5.

The mass spectrometer ion currents were then compared with the Langmuir probe derived ion concentrations to obtain a calibration. This was done by equating, at 10 mm above the burner where the $C_3H_3^+$ ion dominated and the curves were relatively flat, the "sum of the individual ion currents" to the total ion concentration measured by the Langmuir probe in a similar flame.[23] This gave a calibration factor by which all ion currents (resolved individual or high-pass filter totals) were multiplied to give ion concentrations. It can be seen in Fig. 6 that both the current "sums" (of individual peaks) and "totals" (high-pass filter results) are in good agreement throughout the flame, yet they deviate strongly from the Langmuir probe result beyond about 10 mm. The reasons for this deviation are discussed in Section III.D.

III. RESULTS AND DISCUSSION

A. TEMPERATURE EFFECTS

Some measurements of the effect of temperature on soot formation in premixed flames were made, with very surprising results. This work has been published[24] and so it will be only cursorily summarized here with a brief discussion of some of the implications which we have not yet explored. In these experiments soot formation was observed in atmospheric pressure toluene and decalin flames of various fuel/O_2/N_2 mixtures. As the $O_2/(O_2 + N_2)$ ratio was increased, the onset of sooting occurred at higher fuel/O_2 ratios, and at higher calculated flame temperatures, consistent with previous observations of others.[25,26] However, when the temperatures were measured using two-wavelength emission pyrometry, the flame temperatures at the soot thresholds were constant for each fuel (1750 K for toluene and 1720 K for decalin). These results for toluene are displayed in Fig. 7. Soot volume fractions, f_v were also measured under a Naval Research Laboratory contract,[27] using a multiwave-

length laser extinction technique, as a function of equivalence ratio, $O_2/(O_2 + N_2)$ ratio, and the experimental flame temperature. The soot volume fractions varied strongly with the $O_2/(O_2 + N_2)$ ratio, but the variation with measured temperature was independent of the $O_2/(O_2 + N_2)$ ratio. It, in fact, appeared in these experiments that the soot yield, for each fuel, at and above soot threshold was uniquely determined by the measured flame temperature, independent of how this temperature was obtained.

These results clearly indicate the hazards involved in using adiabatic flame temperatures instead of measured temperatures in interpreting soot formation studies. The results in Fig. 7 imply that, as the equivalence ratio is increased, some of the heat release reactions do not go to completion- - other obvious explanations can be rejected.[24]

Probably related to the above is the equilibrium or nonequilibrium nature of soot formation in flames. It is generally accepted that at the threshold for soot formation the production of soot is not predicted by an adiabatic equilibrium calculation but that soot formation requires a nonequilibrium mechanism for its formation. We, in fact, use this as an argument for the ionic mechanism of soot formation which depends upon the nonequilibrium formation of chemi-ions to drive the process. For more recent use of this concept see Refs. 28-30. We have made some equilibrium calculations of the quantity of soot formed in flames at fuel concentrations exceeding the threshold fuel composition, and they seem to predict an excess of soot over that measured. This work needs further evaluation and substantiation before we are willing to report it publicly; if substantiated it would mean completely different mechanisms might be involved in flames near soot threshold and in very rich mixtures!

B. THERMODYNAMICS OF SOOT FORMATION

It has been customary in the combustion community to express the composition of a fuel-oxidizer mixture as an equivalence ratio calculated by assuming the products are H_2O and CO_2. The equivalence ratio is then defined as:

$$\Phi = \frac{(\text{Fuel/Oxidizer})_{\text{ACTUAL}}}{(\text{Fuel/Oxidizer})_{\text{CALCULATED}}}$$

While this is usually satisfactory it has been recognized to be somewhat misleading for fuel rich mixtures, such as encountered in soot work. Some people use the C/O ratio[31,32] and some have chosen to assume the product is CO rather than CO_2.[33] In search of some guidance on how to treat this problem we have calculated the adiabatic equilibrium composition at the soot threshold for a set of fuels spanning the threshold soot index, TSI, range from 0 to 100[34,35]; the results are plotted in Fig. 8. It is clear that CO is no better choice to predict sooting than CO_2 and that H_2O is similarly a poor choice.

The linear variations of the ratios plotted in Fig. 8 are interesting but their significance is not clear; they are probably an important consideration in the equilibrium/nonequilibrium problem poised above!

C. REACTION HEATING OF SOOT PARTICLES

In the ionic mechanism of soot formation it is assumed that the large ions and very small charged soot particles are formed by the growth of smaller ions via the addition of small neutral species, such as acetylene. Homann has proposed[11] an alternate mechanism to explain the observed large ions. He supports the hypothesis that as the incipient soot particles grow, the exothermic growth reactions deposit energy in the particles more rapidly than they can dissipate the energy. The particle temperature thus exceeds the gas temperature so the particles are thermally ionized. Homann has not developed a quantitative description of the phenomena[36]; it is incumbent upon us to analyze this alternate mechanism. This analysis has not yet been published so will be presented here in detail.

We have made quantitative estimates of the amount of reactive heating expected for growing species in a $\phi = 3.0$, 2.67 kPa C_2H_2/O_2 premixed flame (50 cm s^{-1} unburned gas velocity). The model selected is similar to that used by Millikan[37] to estimate particle temperatures. We first describe the model and quantitative estimates of the various input parameters, and then discuss the implications on particle heating.

Growth of species from molecular size (150 amu) to particle size (10^5 amu) is considered. P_n, designates a particle which has undergone n reactive collisions. The particle is heated in the growth reaction with species G,

$$P_{n-1}\,(T_0) \;+\; G \xrightarrow{k_G(n)} P_n\left(T_0 + \frac{q_G}{C_n}\right)$$

where $k_G(n)$ is the reaction rate constant for the process creating P_n. The initial temperature of the precursor, P_{n-1}, is T_0, and the entire exothermicity, q_G, of the reaction is assumed to heat particle P_n of heat capacity, C_n.

Particle cooling occurs either radiatively or by collisions with the flame species, M, as described by the process:

$$P_n(T_i) \;+\; M \xrightarrow{k_M(n)} P_n\left[T_i - \frac{q_M}{C_n}\right] \;+\; M$$

where q_M is the energy transferred to the bath gas, and $k_M(n)$ represents the collision rate constant of M with P_n.

Several properties of the low pressure C_2H_2/O_2 flames lead to simplification of the model. Relative to the range of particle sizes considered here (10 nm diam), the gas mean free path is very large (typically on the order of 10 μm) compared to the particle diameter so molecular heat transfer processes dominate. For simplicity we neglect radiative cooling of the hot particles so that an upper limit to particle heating is obtained.

The reactive heating rate is approximated as the enthalpy of the growth reaction, $\Delta H_\bullet$, times the rate of reactive collisions of the growth species G with the particle: $\Delta H_\bullet\ k_\bullet[G]$. The rate constant, $k_\bullet$, can be written as the product $f_\bullet Z_\bullet[G]$ where $Z_\bullet$ is the collision rate of G with the particle and $f_\bullet$ is the fraction of collisions which are reactive. Similarly, the rate of heat transfer to the flame gases is approximated as $q_M Z_M[M]$ where q_M is the heat transfer per collision between the particle and M, and Z_M is the collision rate. q_M is given by:

$$q_M = \alpha\ C_M\ \Delta T \tag{1}$$

where α is the accommodation coefficient for energy transfer from the particle to M, C_M is the heat capacity of M, and ΔT represents temperature difference between the particle and the flame, $T_p - T_F$.

The competition of these two processes will result in particle heating to a steady-state temperature determined by the condition:

$$\Delta H_\bullet f_\bullet Z_\bullet[G] + q_M Z_M[M] = 0.$$

The particle temperature is then given by:

$$T_p(\infty) = T_F - \frac{\Delta H_G f_G Z_G[G]}{\alpha\ C_M\ Z_M[M]} \tag{2}$$

$T_p(\infty)$ represents the "steady-state" temperature of the particles; the particle "temperature" will initially be a function of time.

We first consider the steady-state particle temperatures for various "particle" sizes from molecular size (150 amu) to 10^5 amu, corresponding to a spherical particle diameter, d_p, of 6 nm (density = 1.5). It will be shown that to a first approximation, $T_p(\infty)$ is independent of the particle size. Thus the particle temperature can be considered independent of its growth history once "steady-state" is reached. The denominator of the right hand term of Eq. (2) is:

$$\alpha C_M Z_M[M] = \sum_i \alpha_i C_i Z_i X_i[M] \tag{3}$$

where the sum is taken over the major flame components with mole fractions X_i, and [M] is the total gas concentration. For the $\phi = 3.0$ flame, the major species are CO, H_2 and C_2H_2 in approximate ratio[5,9] of 6:3:1 and [M] = 1×10^{17} molecules cm^{-3} at 2000 K and 2.7 kPa. The collision number Z_i from kinetic theory is:

$$Z_i = \pi \left[\frac{d_p + d_i}{2}\right]^2 \left[\frac{8kT}{\pi \mu_i}\right]^{0.5} \qquad (4)$$

where μ_i is the reduced mass of the particle/reactant pair. For large particles this smoothly goes over into the rate of molecules i colliding with the surface of a spherical particle,

$$Z_i = \frac{\pi d_p^2}{4} \left[\frac{8kT}{\pi m_i}\right]^{0.5} \qquad (5)$$

Even for a particle of mass 150, use of m_i rather than μ_i results in less than 10% error in the collision number, and the variation in d_i for H_2, CO, and C_2H_2 (0.2-0.4 nm)[38] is small relative to d_p (≈ 1 nm). Assuming α to be independent of the gas, we calculate an effective value for Eq. (3) at 2000 K in terms of the CO diameter, d_{CO}, which will be essentially valid for all particle sizes. The heat capacities used were estimated to be (kJ K^{-1} $mole^{-1}$) 26, 29, and 75 for H_2, CO, and C_2H_2, respectively.[39] Likewise the reaction collision number Z_0 can be simplified. Equation (2) is now (employing $m_0 \approx 26$ amu for acetylene, the only real growth candidate)[40-42]

$$T_P = T_F - \frac{19\,\Delta H_G\, f_G X_G (d_P + d_G)^2 [M]}{\alpha (d_P + d_{CO})^2\, [M]} \qquad (6)$$

where ΔH_0 is in kJ $mole^{-1}$ and the diameters are in angstroms. Assuming $d_0 \approx d_{CO} < d_P$, or when d_P is very large, the size dependence (except any hidden in α) drops out and

$$T_P = T_F - \frac{19(\Delta H_G(\text{kJ mole}^{-1})\, f_G X_G)}{\alpha} \qquad (7)$$

This equation holds equally well for molecules and particles from 150-10^5 amu in a $\phi = 3.0$ flame. Now, in order to evaluate T_P, we need to estimate the heat of reaction which we have assumed involves the major hydrocarbon species, C_2H_2. We note that mass spectrometric measurements in low pressure C_2H_2/O_2 flames have shown that the next most abundant hydrocarbon species, C_4H_2, is an order of magnitude lower in concentration.[5,9]

Mature soot particles show considerable graphitic nature while small, young particles have higher H/C ratios which decrease as the particle grows. We estimate the exothermicity of the growth reactions by two overall processes.

$$C_2H_2 \rightarrow 2C(s) + H_2 \qquad \Delta H_{298} = -227 \text{ kJ mole}^{-1}$$

$$1/4C_6H_6 + C_2H_2 \rightarrow 1/4C_{14}H_{10} + 1/2H_2 \qquad \Delta H_{298} = -178 \text{ kJ mole}^{-1}$$

Using available heat capacity data,[39,43] at 2000 K, the processes have exothermicities of about 210 and 165 kJ mole^{-1}, respectively. Thus Eq. (7) becomes:

$$T_P \leq T_F + \frac{400 f_G}{\alpha} \qquad (8)$$

for the more exothermic process.

The coefficients, f_e and α, remain the major uncertainties as Millikan found.[37]

Energy transfer in reacting molecular systems has been investigated both for thermal and chemically activated systems. The efficiency of energy transfer is expressed in terms of an average energy step based on a model of energy transfer probability. A number of investigations have shown that the mean energy transferred per collision decreases with increasing temperature.[44-46] Particularly apropos to the accommodation coefficient α for present considerations are experiments by Barker and coworkers[45,47] on vibrational energy transfer from highly excited ground electronic state azulene produced in internal conversion of the laser excited molecule. This mimics the exothermic growth process in that the vibrational temperature of the large molecule is much higher than that of the bath gas. Using different wavelengths for excitation, the dependence of the transferred energy on the azulene energy content was probed.[47] The average collisional energy transfer to CO was about 375 cm^{-1} for azulene excitation of 30,600 cm^{-1}, and it was 150 cm^{-1} for 17,500 cm^{-1} excitation. These values correspond to $\alpha \approx 0.2$ and 0.1 for CO in the high and low energy excitations, respectively. The corresponding values (energy transferred and α) for H_2 (about the same heat capacity as CO) were roughly half of these. Barker and Golden[45] found roughly a $T^{-0.5}$ dependence for the average energy transferred to the diatomic N_2 in the azulene system. In the range 300-525 K it was about 295 cm^{-1} at room temperature, and it dropped to 180 cm^{-1} from 400 to 525 K in good agreement with the observations of Brown et al.[46] for N_2 in ethyl acetate from 300-800 K. Also, Heymann et al.[48] found the average energy transferred to CO from cycloheptatriene to exhibit a roughly $T^{-0.5}$ dependence while other monatomic and diatomics exhibited somewhat lower temperature dependencies. Considering the major post flame compo-

nent CO, we correct the conservative $\alpha = 0.1$ to flame temperatures by scaling by the inverse square root of the temperature which gives $\alpha \approx 0.04$.

Gas-surface accommodation coefficients, f_e, are generally fairly high at room temperature (0.3-1) and also have been observed to decrease with increasing temperatures. In a study of gas-surface single-collision energy transfer, Rabinovitch and coworkers[49] found a vibrational accommodation coefficient of 0.2 for cyclobutene on quartz at 975 K. We assume that α for the particles is at least as large as the molecular value of 0.04 estimated above.

The particle growth rate is obtained from the electron microscopic studies by Howard and coworkers.[6] From their results they calculated surface growth rates for soot particles in the "standard" acetylene-oxygen flame ($P \approx 2.7$ kPa, $u = 50$ cm/s) below about 2.5 μm/s. This corresponds with an estimated value of f_e on the order of 0.01 for C_2H_2 as the growth species. This compares with a maximum value of $f_e = 0.001$ (for C_2H_2) from the atmospheric pressure flame measurements of Harris and Weiner.[40-42]

Substituting $\alpha = 0.04$ and $f_e = 0.01$ in Eq. (8) gives a temperature for the particle 100 K greater than the gas temperature. If we increase the measured gas temperature by 100 K and calculate the total ion concentration using Saha's equation the results reported in Fig. 9 are obtained. The small increase in equilibrium concentration of charged particles still gives a theoretical concentration below the experimental value. The most dramatic difference between the experimental measurements and the calculated values occurs at small distances from the burner. Here the measured ion concentration is falling while the calculated value is rising.

The above analysis neglects the possible formation of negative particles by electron attachment by the equilibrium

$$P + e^- \rightarrow P^-$$

It has generally been considered that the ions are predominantly positively charged but both Homann[50] and we[23] have presented evidence for negative ions in this flame. If the concentration of negative ions is assumed to be in equilibrium with the neutral particles that process will remove electrons from the system throwing the thermal ionization reaction

$$P \rightleftharpoons P^+ + e^-$$

further to the right, creating more positive ions. This has yet to be considered on a quantitative basis; we will do so before we publish. The decrease in the measured value with distance is consistent with the picture that the ions are formed in the flame front by chemi-ionization and then disappear by ion-electron recombination. At further distances from the burner the measured and calculated charged particle concentrations may agree because when the particles become larger thermal equilibrium ionization prevails. This is completely different from the ionization we are concerned about in the earlier

part of the flame; unfortunately the two parts of the flame are often confused.

The results reported in Fig. 9 do not support Homann's proposal.[11] We are not as confident as we would like to be however with the values of α and f_e so have held up publication until we can find more reliable values.

D. ACETYLENE-OXYGEN FLAMES

1. Total Ion Concentrations

Figure 6 shows a great disparity between the ion concentrations measured by the mass spectrometer and by the Langmuir probe at distances greater than 10 mm. This is due to the formation, beyond this point in the flame, of large ions which are measured by the Langmuir probe but not by the mass spectrometer. The median ion mass which we previously deduced[23] for this flame from Homann and Stroefer's measurements,[50] Fig. 10, shows an extremely sharp increase, from 55 to 4,500 amu, between 10 and 15 mm distance above the burner and to 35,000 amu at 25 mm distance. These large ions are not detected by our mass spectrometer. Soot (defined as particles with a diameter greater than 1.5 nm which are detectable by electron microscopy) first appears at 20 mm above the burner and peak in concentration, off scale, at 35 mm.[4,15] These particles are located too far downstream to be considered the precursors of the relatively small ions observed here (see also Ref. 1).

2. Ion Spectra and Mechanistic Implications

From the ion spectra at various distances above the flame we note that the ion concentrations decay with distance above the burner, with the larger ions increasing in relative concentration, and the initial ion, $C_3H_3^+$ (39 amu), becoming less dominant. The most common spacing between adjacent ions is 12 amu, equivalent to the addition of a carbon atom.

The occurrence of carbon and hydrogen in the observed ions is shown in Table II. The masses of the ions $C_xH_y^+$ increase in a sequence where x is an integer increasing from 3 to 45 and where y is an odd integer increasing from 3 to 17 for the ions with the highest C/H values. The ions appear to increase in mass by adding simple carbon atoms while maintaining a fixed number of hydrogen atoms up to a specific C/H ratio at which two hydrogens and a carbon atom are added simultaneously. Clearly this sequence does not represent a series of elementary chemical reactions but a sequence of observed species which must be accounted for by a set of elementary reactions. This we will do below.

In Table II, all of the ions contain an odd number of hydrogen atoms. As shown in Table I, the even carbon number ions have protonated structures while the odd carbon number ions are molecular ions. It has been argued by Stein[51] that the protonated-benzenoid-polyaromatic-hydrocarbons (BPAH.H+) ions, with an even number of carbon atoms, are in equilibrium with

the unprotonated ion and a hydrogen atom:

$$BPAH\text{-}H^{\dagger} \rightleftharpoons BPAH\cdot^{\dagger} + H\cdot \qquad (9)$$

We observe the protonated species which Stein claims should only exist at temperatures below 1500 K; the temperatures in our flame were greater than 1500 K. Stein attributes our observation of the protonated species to the rapid rate of Reaction (9) to the left in the cooled flame gases near the sampling cone. This equilibrium, if important (we are not convinced that it is) does not alter the arguments presented here or those for the ionic mechanism of soot formation. The important point is that large molecular ions are observed and their source must be accounted for. The reactions we propose explain their production. The above equilibrium would only add an additional set of reactions to the mechanism, and some of the ion addition reactions would involve the unprotonated molecular ion rather than the protonated molecule. Stein's argument, based on rapid ion molecule equilibria, supports our premise that ion-molecule reactions in flames are very rapid.

Stein did not treat the corresponding case for odd-carbon numbered carbon ions, which we find to be unprotonated.

The set of ions in Table II can be used to define the types of reactions which might be involved. The most obvious reactants with $C_3H_3^+$ are acetylenes and our original reaction schemes included[2,52] :

$$C_3H_3^+ + C_2H_2 \rightarrow C_5H_3^+ + H_2$$
$$C_3H_3^+ + C_4H_2 \rightarrow C_7H_5^+$$
$$C_7H_5^+ + C_2H_2 \rightarrow C_9H_7^+$$
$$C_9H_7^+ + C_2H_2 \rightarrow C_{11}H_7^+ + H_2$$

These types of reactions account for the odd numbers of carbon atoms and the removal of two hydrogen atoms; thus ions of the general formula $C_xH_{N-2}^+$, $C_xH_{N-4}^+$ where N is an odd integer are observed. As the ion masses increase there is a general increase in the C/H ratios up to 2.6 in $C_{45}H_{17}^+$.

The addition of polyacetylenes, C_4H_2, C_6H_2, and C_8H_2 (the last two reported in Ref. 53) account for the increased C/H ratio; thus reactions of the type

$$C_9H_7^+ + C_4H_2 \rightarrow C_{13}H_9^+$$
$$C_{13}H_9^+ + C_6H_2 \rightarrow C_{19}H_{11}^+$$

or

$$C_{15}H_{11}^+ + C_4H_2 \rightarrow C_{17}H_{11}^+ + C_2H_2$$

increase the C/H ratio. The last reaction effectively adds two carbon atoms without changing the number of hydrogen atoms. This reaction type was included in an earlier proposed ion-molecule mechanism of soot formation.[52] Interestingly, Warnatz et al.[54] in studies of a similar flame point out that about 35% of the C_2H_2 reacts via C_4H_2. Michaud et al.[7] deduced equilibrium con-

stants and heats of formation of ions from flame measurements assuming the above type equilibria. Bittner and Howard[55] suggested that such ion-molecule reactions are responsible for the equilibrium between acetylene and diacetylene.

We conclude from the above discussion that polyacetylenes must be considered as important reactants in the ion-molecule growth of large ions in flames.

We have yet to account for the even number of carbon atoms observed; all of the reactions above, starting with $C_3H_3^+$, lead to an odd number of carbon atoms. Reactions of the type:

						ΔH_{298}, kJ/mol
$C_3H_3^+$	+	$CH_2{=}C{=}CH_2$	----→	$C_4H_3^+$	+ C_2H_4	- 37
			----→	$C_4H_5^+$	+ C_2H_2	- 144
			----→	$C_6H_5^+$	+ H_2	- 218
$C_3H_3^+$	+	$CH_3{-}C{\equiv}CH$	----→	$C_4H_3^+$	+ C_2H_4	- 30
			----→	$C_4H_5^+$	+ C_2H_2	- 137
			----→	$C_6H_5^+$	+ H_2	- 211

must thus be important.

Some of the above reactions have been observed (for linear $C_3H_3^+$) at near room temperature.[56,57] We will examine below whether their rates in flames are sufficient to account for the large observed molecular ions.

3. Ion and Neutral Species Profiles and Reaction Rate Implications

Individual ion profiles are presented in Fig. 11. Neutral species profiles from Bittner and Howard,[55] Delfau and Vovelle,[9] and Laurendeau[58] are plotted in Fig. 12 along with selected ion profiles from this study. In general, the data of Bittner and Howard and of Delfau and Vovelle are in excellent agreement; where they disagreed, we report a mean value, see Fig. 12 caption.

A number of observations are immediately apparent in Fig. 12. Most striking is the low concentration of ions relative to neutral species. With the exception of C_4H_2, all of the neutrals reach their peak concentrations earlier than the ion concentration peaks; C_4H_2 peaks at about the same position as ions. The ion concentrations decay more rapidly than do the neutrals; some of the neutrals, in fact, increase in concentration with distance. These increases in concentration continue far downstream beyond where soot particle

formation ceases, thus eliminating reactions of these polycyclic aromatics with acetylenes as soot precursors[2,59] because their rate of soot formation would remain high beyond where soot ceases to be produced. Thus, for example:

$$\text{Rate} = k[C_2H_2][C_{14}H_8]$$

would not change through the position in the flame where soot is no longer formed unless the slight temperature decrease greatly lowers k. In contrast, the coincidence of rapid decay in ion concentrations, especially larger ions,[23] with the observed increase in soot concentration is consistent with an ion-molecule mechanism of soot formation.

Another striking difference between neutral species concentrations, Fig. 12, and ions is the large decrease in neutral species concentrations with increasing mass compared to that for ions. For example, the change in concentration from a C_3 neutral to a C_{14} neutral is greater than three orders of magnitude. A similar change in ion mass occurs with about one order of magnitude change in concentration; the ions change from C_3 to C_{45} ions with only a two order of magnitude change in concentration. This might be interpreted as indicating a slower rate of growth for neutral species than for ions. Thus, if the concentration of large neutral species is extrapolated from the available neutral species concentrations, one would conclude that large neutral species concentrations are, in fact, less than concentrations of equivalent sized ions! An extension of this type of argument leads, for both species, to concentrations far less than the concentration of soot particles! For ions, we know that the total ion concentration, when very large ions are included, see Fig. 6, is much greater than the concentrations of ions reported in Figs. 11 and 12, and that the total number of ions is comparable to the concentration of soot particles, see Ref. 23. Equivalent evidence for neutral species is not so definitive (see e.g., Ref. 10).

All of the ions, with few exceptions, peak at the same position in the flame. This is true for both even and odd carbon number ions independent of the suggested structure. This can occur only if an equilibrium exists among all of the ions, or if the rate of production of large ions is rapid compared to the time scale of the experiment. In nonsooting flames the appearance of many ions early in the flame has been interpreted as due to equilibrium.[60] This again implies rapid ion-molecule reactions at flame temperatures, even for large ions. The demonstration that such ion-molecule reactions are rapid in flames is significant because there are few actual measurements of ion-molecule reaction rate coefficients as a function of temperature[61-63] and to our knowledge none at flame temperatures.

Ion-molecule forward rate coefficients for nonpolar molecules can be calculated by the Langevin equation, which does not have a temperature dependence[61,63]:

$$k_c = 2\pi e \left(\frac{\alpha}{\mu}\right)^{1/2}$$

where: e = charge on ion, α = polarizability of the neutral species, and μ = reduced mass.

Measurements for $C_3H_3^+$ reacting with several species,[56,57,64] at near room temperature are in agreement with Langevin theory for the linear isomer of $C_3H_3^+$ (Table III); the cyclic structure is more stable and reacts more slowly. These two structures are assumed to be in rapid equilibrium at flame temperatures, the linear reforming as it is removed by ion-molecule reactions. There is some evidence in the measurements of Eyler[57] that larger ions and larger molecules have lower rate coefficients than predicted by the Langevin equation (Table III). Eyler and associates[65] have recently obtained data which indicate that the reaction of $C_3H_3^+$ with C_2H_2 is much slower at room temperature than previously reported. This does not represent a problem to the ionic mechanism of soot nucleation; there seems to be sufficient concentration of polyacetylenes and other reactants available to account for the required rates of ion growth, see Table III. Arguments have been made that ion-molecule reactions are too slow at flame temperatures to be important in soot formation. The rapid "equilibrium" among a large range of ions indicated by the results in Fig. 11 strongly refutes this claim.

The profiles reported in Fig. 11 were used to estimate the rate coefficients for the possible reactions involved in forming or destroying the observed ion. Reactions thus obtained from the profiles which give reasonable rate coefficients with an assumed neutral reactant partner are considered important candidates in determining the observed profiles. However, we first considered the extent to which diffusion influences the profiles.

The rate of increase of ion concentration in the flame front was used to estimate a characteristic distance, L, and a characteristic time, τ. The time was calculated directly from the total gas flow velocity, correcting for temperature and molar changes due to reaction.

The effective diffusion coefficient, D_+, was then calculated from:

$$D_+ = \frac{L^2}{\tau}$$

The characteristic dimensions of the experiment are taken from the characteristic dimension of a cylinder[66]:

$$\left(\frac{1}{L}\right)^2 = \left(\frac{\pi}{H}\right)^2 + \left(\frac{2.405}{R}\right)^2$$

where H is the height of the cylinder and R = radius. H is taken as the thickness of the profile of the species of interest at half the maximum concentration; 0.4 cm was used for all ions--certainly within the accuracy of the estimate. R was taken as the burner radius. These measured ion diffusion coefficients from our experiments are plotted against ion mass as points in

Fig. 13 and these are compared with ion diffusion coefficients calculated from the ion mobilities, μ_+ by the Einstein relation[67]:

$$D_+ = -\left(\frac{k}{e}\right) \mu_+ T$$

where: k = Boltzmann constant and the ambipolar diffusion coefficient, $D_a \approx 2D$. The actual value is expected to fall between these two curves, depending upon the extent of negative ion formation.

The agreement between experimental and calculated characteristic diffusion times, in both the magnitude and shape of the curve is surprisingly good. This tends to confirm the mass calibration of the mass spectrometer. The two points that fall farthest outside the calculated area are $C_3H_3^+$ at mass 39 and $C_{10}H_9^+$ (a six-numbered ring with a four carbon side chain). The $C_3H_3^+$ deviation probably relates to its being the initial ion. The reason for the deviation of $C_{10}H_9^+$ is not clear.

From the above it is clear that diffusion dominates the shape of the concentration profiles in the flame front. The characteristic ion-molecule reaction times must therefore be small compared to diffusion times. Recognizing this, we screen candidate reactions involved in the ion growth process by estimating a minimum value of the rate constant for the candidate reactions based on the observed characteristic times and reactant concentrations. These values are compared with estimated (Langevin equation) and experimentally observed rate constants for some typical candidate reactions in Table III.

Average characteristic times decrease with increasing ion mass, Fig. 13: 0.55 ms from 39-153 amu, 0.36 ms for 165-253 amu, 0.27 ms from 277-375 amu, and 0.25 ms for 387-509 amu. Again, there is no significant difference between odd and even carbon number ions in the same mass range. We estimated required rate constants (to be faster than diffusion) based on a conservative value of the characteristic time, 0.5 ms, assuming a bimolecular reaction in which the neutral reactant, n, is in excess:

$$k = \frac{\ln 2}{\tau\, n}$$

We consider two basic reaction schemes by which large ions might be produced. In the first scheme a large neutral molecule reacts with a small ion to produce a large ion, e.g.:

$$C_{16}H_{10} + C_3H_3^+ \rightarrow C_{19}H_{11}^+ + H_2$$

In the second scheme a small neutral species reacts with an ion to produce a larger ion, e.g.:

$$C_4H_2 + C_{17}H_{11}^+ \rightarrow C_{19}H_{11}^+ + C_2H_2$$

These examples, in fact, represent two competitive routes used to explain the formation of large ionic species. Are the large ions formed by the growth of

neutral species such as the first reaction, with subsequent additions of small ions to these large neutrals; or are the large ions formed by the addition of small species such as acetylene and diacetylene to large ions, our proposed mechanism of soot formation via ion-molecule reactions?[2,3,52,68] We are interested here in deciding between these alternate mechanisms for producing the large molecular ions which are observed in flames.

The low limits to the ion molecule rate constants (calculated from the characteristic time, concentration of neutral reactant, and the half-life equation) required for the chemical reactions to be faster than the diffusion process are presented in Table III. They span 7 orders of magnitude. For the smaller neutrals reacting with $C_3H_3^+$ the agreement, Table III, between experiment and Langevin theory is excellent; for $C_{10}H_8$ to $C_{14}H_8$ the experiment gives a smaller value than theory. Clearly reactions of ions with acetylene and diacetylene are possible sources of large ions; only very modest rate coefficients are required. At the other end of the scale, reactions of large neutrals with small ions are ruled out by the unreasonably large rate coefficients that would be necessary. This occurs because of the large change in the concentration of the neutral reactant, n, in the denominator of the above equation for k when large molecule concentrations replace the concentrations of C_2H_2 and C_4H_2. One can, in fact, generalize that only reactants, in which one of the partners is in large supply, can be effective in soot producing reactions.

For reactions of small ions with the large neutral species the data in Table III demonstrate that measured and calculated reaction rate coefficients are far lower than those required to account for the experimental observations; for reactions of large ions with small neutral species the measured and calculated reaction rate coefficients are adequate to account for the experimental observations. Thus it is concluded that large ions are not produced by addition of small ions to large molecules but rather by reactions of large ions with small molecules. Examination of the data for small neutral molecules reacting with large ions reveals that there are many small molecules, including benzene, which are excellent candidates for adding to large ions. This is consistent with the observation of rapidly growing ions. Thus the proposed mechanism[2,3,52,68] of ion growth by addition of species such as C_2H_2 and C_4H_4 to form larger ions is confirmed. Coupled with previous arguments,[2,3,15,23,52,68] this is additional strong evidence that the mechanism of soot nucleation is through a series of very rapid ion-molecule reactions.

E. BENZENE-OXYGEN FLAMES

Ion concentration profiles were obtained in the same benzene/oxygen/30% argon flames in which Bittner and Howard[5] measured neutral species profiles. The objective was to increase the data base against which detailed modeling studies could be performed and to compare the ion profiles in acetylene and benzene flames. The same burner was used as used by Bittner and Howard to

assure as close a comparison of the data as possible, see Section II.B. A fuel rich but nonsooting flame at $\Phi = 1.8$ and a sooting flame at $\Phi = 2.0$ were studied. The total pressure was 2.7 kPa and the total unburned gas flow velocity was 50 cm/s. These data have not been interpreted and the mass spectrometer ion profiles have not been reduced to absolute concentrations. The results are recorded here for archival purposes; as soon as time and funds are available they will be interpreted in terms of the mechanism of ion formation in flames and the participation of ions in the mechanism of soot formation.

1. Total Ion Concentrations

The total ion concentrations in both flames were determined by Langmuir probe (0.65 cm long, 0.025 cm diam Pt/10% Rh wire) measurements. Two techniques were employed. In one the probe current was measured at a fixed negative voltage of - 20 V and the data interpreted according to the theory of Clements and Smy[69]. The other technique was to measure complete current/voltage curves from -60 V to +18 V and from these curves obtain the probe current at the plasma potential from which the positive ion concentration was calculated by Calcote's probe analysis.[70] The currents collected at -20 V for these current/voltage curves at a fixed distance agreed with the current profiles collected at constant -20 V. Complete current/voltage curves were obtained with the hope of obtaining electron concentrations and, from the wall potential, the mass of the positive ions. Neither of these analyses were successful; possibly more effort would yield useful results.

The probe currents at -20 V and at the plasma potential, both extrapolated from I/V curves, are plotted in Fig. 14 for the $\Phi = 1.8$ flame along with the positive ion concentration derived by the two respective interpretations. The differences in derived concentrations are greater than normal. The higher result obtained from the -20 V data is probably the more reliable, because of problems with this set of data in deriving a plasma potential. Because we do not know the variation in ion mass through the flame we have arbitrarily assumed a mass of 39 amu in reducing the data; the use of a larger mass would increase both sets of ion concentrations but would increase the lower concentration curve more than the higher set because ion mass has a greater effect on the interpretation by Calcote than the interpretation by Clements and Smy. In reducing the probe data the flame temperatures measured by Bittner and Howard[5] by radiation corrected thermocouples were used, Fig. 15.

Probe currents measured at - 20 V in the $\Phi = 2.0$ flame are reported in Fig. 16. These will be subsequently reduced to obtain positive ion concentrations.

Total ion concentrations above a given mass were obtained with the mass spectrometer by operating the instrument as a high pass mass filter. This is done by turning the dc voltage on the quadrupole off so that all ions above a given mass are detected, ions below this mass are rejected. Data for the $\Phi = 1.8$ and $\Phi = 2.0$ flames are presented in Figs. 17 and 18, respectively.

The ion concentration, measured as ion current, by the mass spectrometer and by a Langmuir probe, compare Figs. 17 with 14, and Figs. 18 with 16, are very similar in shape. They are thus presumably measuring the same ion concentrations. This is in complete contrast to the experiments with an acetylene/oxygen flame, Fig. 6, where the ion concentration measured with the mass spectrometer was much lower than that measured with a Langmuir probe. The difference was about 300. Why this great difference between benzene and acetylene? In the acetylene experiment we argued that the mass spectrometer could not detect large ions while the probe could detect very large ions and thus the difference was due to the formation in the flame of very large ions which went undetected by the probe. Application of this reasoning to the benzene flame leads to the conclusion that there are very few large ions in this benzene flame. This is consistent with observations by Homann[50,71] from a completely different experiment.

The significance of this difference between the two flames for understanding the mechanism of ion formation in fuel rich flames and the role played by ions in soot formation will have to await more detailed analyses. Two basic questions, which may be related, are: why do the ions not grow and why is their rate of recombination different? If the ions do not grow, their recombination coefficients will be greater, so they will decay more rapidly. Or, if the number of negative ions is greater in the acetylene flame than in the benzene flame the recombination rate will be greater in the benzene flame. Under such conditions the ions in the benzene flame might disappear by recombination before they have a chance to grow. We have demonstrated dramatic changes in the recombination coefficient for acetylene flames near soot inception which substantiates this argument. Homann,[50] however, reports that in a benzene and acetylene flame producing equal concentrations of soot the total number of positive and negative ions in each flame is about equal and the benzene flame has about twice as many total ions as does the acetylene flame. He also reports a completely different distribution of negative ions with respect to mass in the two systems.

How the observation that there are no large ions in sooting benzene/oxygen flames affects the arguments for the ionic mechanism of soot formation is not clear. The rapid disappearance of moderately sized ions to form neutral species which then grow to soot particles would certainly be reasonable. The main contribution of the ionic mechanism of soot formation is in the initiation steps and especially to account for the rapid formation of polycyclic species. It would be useful to have large neutral species concentrations in these two flames just like we have information of concentrations for large ions. More detailed quantitative comparison between the acetylene and benzene systems could pay big dividends in understanding the mechanism of ion formation in these systems and the role of ions in soot formation. The addition of a saturated hydrocarbon to the systems studied would greatly enhance the value of this analysis. It would also be of great value to have more quantitative information on negative ions in these chemical systems.

2. Calibration of Mass Spectrometer Sensitivity

The mass spectrometer change in sensitivity with mass was determined by comparing the change in ion current when the dc was off with the sum of the peak individual ion currents over the same mass range. These data were taken in the mass scan mode of the mass spectrometer, i.e., the burner to mass spectrometer sampling cone distance was fixed and the rf voltage on the quadrupole was varied to scan a mass range; this gave the individual ion peaks at a given distance. The dc off data were obtained by setting the dc off at specific rf voltages corresponding to ions above a given mass. A plot of these data against mass permitted the change in current to be obtained for a given mass range. The results are plotted in Fig. 19. These corrections have not yet been applied to the data reported below.

3. Mass Spectra

Ion profiles through the flame for the $\emptyset = 1.8$ flame were obtained by first sweeping the mass at a range of distances and observing the ion spectra at each distance. These data were then used to identify the ion masses. Then the mass spectrometer was set on a specific mass and the burner moved vertically with respect to the sampling cone producing individual ion profiles for each mass. These data are presented in Figs. 20-24 which are organized by increasing mass.

The masses all peak at very nearly the same distance from the burner just as in the acetylene flame. The distances at which the peaks appear are plotted as a function of ion mass in Fig. 25. Some of the masses show double peaks; these are also indicated in Fig. 25. It is interesting that when double peaks appear the extra peak precedes the "regular" peak. The mechanism of formation of dual peaks remains a mystery. The maximum ion current decreases with increasing mass as indicated in Fig. 26.

Fewer ion profiles were obtained in the $\emptyset = 2$ flame because of difficulties with clogging of the ion sampling orifice. These results are presented in Fig. 27. Again dual peaks were observed. The $C_3H_3^+$ ion does not appear until late in the flame and then it is the dominant ion. An explanation of these data is not obvious. The results are consistent with previous results we reported earlier on a slightly different benzene/oxygen flame.[68]

IV. PUBLICATIONS

The following papers have been published based upon work done on this contract:

1. "Ionization and Soot Formation in Premixed Flames," D.G. Keil, R.J. Gill, D.B. Olson, and H.F. Calcote, Twentieth Symposium (International) on Combustion (The Combustion Institute, Pittsburgh, 1985) p. 1129.

2. "The Effect of Temperature on Soot Formation in Premixed Flames," D.B. Olson and S. Madronich, Combust. Flame 60, 203 (1985).

3. "Ion Concentrations in Premixed Acetylene-Oxygen Flames Near the Soot Threshold," D.G. Keil, R.J. Gill, D.B. Olson, and H.F. Calcote, in The Chemistry of Combustion Processes, T.M. Sloane, Ed., ACS Symposium Series 249 (American Chemical Society, Washington, DC, 1984) p. 33.

The following papers have been submitted for publication:

1. "Ion-Molecule Reactions In Acetylene-Oxygen Flames" H. F. Calcote and D. G. Keil, submitted to Combustion and Flame.

2. "Are Ions Important in Soot Formation?" H. F. Calcote, D. B. Olson and D. G. Keil, to be presented at the Fuel Division Symposium, Fall ACS Meeting, August 1987.

3. "Why Does Soot Inception Stop?" H. F. Calcote, submitted to Combustion and Flame.

The following manuscripts are in preparation:

1. "Langmuir and Thermocouple Probe Measurements in Sooting Flames," D.G. Keil, R.J. Gill, D.B. Olson, and H.F. Calcote..

2. "Reaction Heating of Soot Particles," D.G. Keil and H.F. Calcote.

3. Comments on "Effects of Oxygen on Soot Formation in Methane Diffusion Flames," by K. Saito, F.A. Williams and A.S. Gordon, Combust. Sci. Techn. 47, 117 (1986), H.F. Calcote.

4. "Ionization in Near Sooting and Sooting Benzene-Oxygen Flames," D.G. Keil and H.F. Calcote.

V. PERSONNEL

In addition to the authors the following personnel made significant contributions to this program:

Douglas B. Olson, Physical Chemist
Robert J. Gill, Physical Chemist
John C. Pickens, Technician
Helen Rothschild, Librarian and Technical Editor
(Ms. Rothschild also assisted with data reduction.)
Evangeline Stokes, Technical Typist

VI. TECHNICAL INTERACTIONS

Technical interactions with other members of the scientific community have taken several forms, the foremost being presentation of our work at scientific meetings, seminars, and workshops. Proposals and manuscript reviews, an important interaction, require an increasing effort. Personal contacts with other technical people in this field have been maintained by attending meetings, and by correspondence and phone calls. Olson and Calcote visited Dr. Charles Martel at Wright Field to discuss our work, especially the effect of fuel molecular structure on jet engine performance.

The following people visited AeroChem during this contract to discuss the mechanism of soot formation at a workshop sponsored by the Army Research Office:

T. Brabbs and E. Lezberg (NASA/Lewis Research Center)
J. Eyler (University of Florida
W. Flower (Sandia National Laboratories)
M. Frenklach and T. Lester (Louisiana State University)
I. Glassman, A. Gomez, and G. Sidebotham (Princeton University)
S. Harris (General Motors Research Laboratories)
R. D. Kern (University of New Orleans)
W. G. Mallard and R. Santoro (National Bureau of Standards)
D. Mann (U.S. Army Research Office)
J. Tishkoff (Air Force Office of Scientific Research)

The following presentations were made based upon work done on this contract:

1. "Soot Formation in Combustion," H.F. Calcote, Seminar, Stevens Institute of Technology, Hoboken, NJ, 9 February 1983.

2. "Ion Concentrations in Premixed Acetylene Flames," D.G. Keil, R.J. Gill, and D.B. Olson, Chemistry of Combustion Processes Symposium, 185th National Meeting, American Chemical Society, Seattle, WA, 20-25 March 1983.

3. "Ionic Mechanisms of Soot Formation in Flames," H.F. Calcote and D.B. Olson, AFOSR Contractors Meeting on Airbreathing Combustion Dynamics Research, Scottsdale, AZ, 19-23 September 1983.

4. "Use of Langmuir Probes in Low Pressure Sooting Flames," D.G. Keil and R.J. Gill, Fall Technical Meeting, Eastern Section: The Combustion Institute, Providence, RI, 8-10 November 1983.

5. "Ionic Structure of Sooting Flames," H.F. Calcote, R.J. Gill, D.G. Keil, and D.B. Olson, Fall Technical Meeting, Eastern Section: The Combustion Institute, Providence, RI, 8-10 November 1983.

6. "An Ionic Mechanism of Soot Formation in Flames," H.F. Calcote, Invited Presentation, American Physical Society Meeting, Detroit, MI, 26-30 March 1984.

7. "Ionic Mechanism of Soot Formation - Toward a Quantitative Model," H.F. Calcote, NBS Workshop on Flame Radiation and Soot, Gaithersburg, MD, 10 May 1984.

8. "Ionic Mechanisms of Soot Formation in Flames," H.F. Calcote, AFOSR/ONR Contractors Meeting in Combustion, Carnegie-Mellon University, Pittsburgh, PA, 20-21 June 1984.

9. "The Effect of Temperature on Soot Formation in Premixed Flames," D.B. Olson and S. Madronich, AeroChem Soot Workshop, Princeton, NJ, 13 July 1984.

10. "Ionic Theory of Soot Formation," H.F.Calcote, AeroChem Soot Workshop, Princeton, NJ, 13 July 1984.

11. "Ionization and Soot Formation in Premixed Flames," D.G. Keil, R.J. Gill, D.B. Olson, and H.F. Calcote, Twentieth Symposium (International) on Combustion, University of Michigan, Ann Arbor, MI, 12-17 August 1984.

12. "Soot Formation in Flames" Presented by H.F. Calcote to six separate groups on a "People To People" tour through China in which Calcote was the Delegation Leader, 9-30 October 1984.

13. "The Effect of Temperature on Soot Formation in Premixed Flames" D.B. Olson, Eastern Section: The Combustion Institute, Fall Technical Meeting, Clearwater, FL, December 1984.

14. "The Role of Ions and Charged Particles in Soot Formation" H. F. Calcote, Seminar Rutgers University, Engineering and Aerospace Dept., 10 April 1985

15. "An Ionic Mechanism of Soot Formation in Flames" H.F. Calcote, Invited Presentation at the Particle Emission Technology Meeting", Naval Postgraduate School, Monterey, CA, 16-18 April 1985

16. "Ionic Mechanisms of Soot Formation in Flames," H.F. Calcote, Invited Speaker, Gordon Conference, New Hampshire, July 1985.

17. "Are Ions Important in Soot Formation?" H.F. Calcote, Seminar, Princeton University, 18 February 1986.

18. "Ionic Mechanisms of Soot Formation," H.F. Calcote, AFOSR Meeting, Stanford University, California, 18-20 June 1986.

19. "Ion-Molecule Reactions in Sooting Acetylene-Oxygen Flames," H.F. Calcote and D.G. Keil, Eastern Section: The Combustion Institute, Fall Technical Meeting, Puerto Rico, 15-17 December 1986.

VII. INVENTIONS AND PATENT DISCLOSURES

There were no inventions or patent disclosures to report during this period.

VIII. REFERENCES

1. Calcote, H.F., in Soot in Combustion Systems and Its Toxic Properties, J. Lahaye and G. Prado, Eds. (Plenum Press, New York, 1983) p. 197.

2. Calcote, H.F. Combust. Flame 42, 215 (1981).

3. Howard, J.B., Wersborg, B.L., and Williams, G.C., Faraday Soc. Symp. 7, 109 (1973).

4. Wersborg, B.L., Yeung, A.C., and Howard, J.B., Fifteenth Symposium (International) on Combustion (The Combustion Institute, Pittsburgh, 1975) p. 1439.

5. Bittner, J.D. and Howard, J.B., in Particulate Carbon: Formation During Combustion, D.C. Siegla and G.W. Smith, Eds. (Plenum Press, New York, 1981) p. 109.

6. Wersborg, B.L., Howard, J.B., and Williams, G.C., Fourteenth Symposium (International) on Combustion (The Combustion Institute, Pittsburgh, 1973) p. 929.

7. Michaud, P., Delfau, J.L., and Barassin, A., Eighteenth Symposium (International) on Combustion (The Combustion Institute, Pittsburgh, 1981) p. 443.

8. Delfau, J.L., Michaud, P., and Barassin, A., Combust. Sci. Tech. 20, 165 (1979).

9. Delfau, J.L. and Vovelle, C., Combust. Sci. Tech. 41, 1 (1984).

10. Homann, K.H., Twentieth Symposium (International) on Combustion (The Combustion Institute, Pittsburgh, 1985) p. 857.

11. Homann, K.H., Ber. Bunsenges. Phys. Chem. 83, 738 (1979).

12. Homann, K.H., Strofer, E., and Wolf, H., in Combustion Problems in Turbine Engines, AGARD Conference Proceedings No. 353, January 1984, p. 19-1.

13. Homann, K.H. and Schweinfurth, H., Ber. Bunsenges. Phys. Chem. 85, 569 (1981).

14. Howard, J.B., MIT, Personal communication.

15. Keil, D.G., Gill, R.J., Olson, D.B., and Calcote, H.F., in Chemistry of Combustion Processes, T.M. Sloane, Ed., ACS Symposium Series 249 (American Chemical Society, Washington, DC, 1984) p. 33.

16. Hayhurst, A.N. and Kittelson, D.B., Combust. Flame 28, 301 (1977).

17. Kent, J.H., Combust. Flame 14, 279 (1970).

18. Kaskan, W.E., Sixth Symposium (International) on Combustion (Reinhold Publishing Corp., New York, 1957) p. 134.

19. Bradley, D. and Matthews, K.J., J. Mech. Engn. Sci. 10, 299 (1968).

20. Reid, R.C. and Sherwood, T.K., The Properties of Gases and Liquids, 2nd ed. (McGraw-Hill, New York, 1966) Ch. 9 and 10.

21. Bonne, U. and Wagner, H.Gg., Ber. Bunsenges. Phys. Chem. 69, 35 (1965).

22. Calcote, H.F. and Keil, D.G., "Ion-Molecule Reactions in Sooting Acetylene-Oxygen Flames," AeroChem TP-454A, submitted to Combust. Flame.

23. Keil, D.G., Gill, R.J., Olson, D.B. and Calcote, H.F., Twentieth Symposium (International) on Combustion (The Combustion Institute, Pittsburgh, 1985) p. 1129.

24. Olson, D.B. and Madronich, S., Combust. Flame 60, 203 (1985).

25. Street, J.C. and Thomas, A., Fuel 34, 4 (1955).

26. Millikan, R.C., J. Phys. Chem. 66, 784 (1962).

27. Naval Research Laboratory, Contract No. N00014-83-C-2311.

28. Harris, S.J., Combust. Flame 66, 211 (1986).

29. Frenklach, M., Clary, D.W., Yuan, T., Gardiner, W.C., and Stein, S.E., Twentieth Symposium (International) on Combustion, (The Combustion Institute, Pittsburgh, 1984), p. 87.

30. Calcote, H.F., "Why Does Soot Inception Stop?" AeroChem TP-464, submitted to Combust. Flame as Brief Communication.

31. Homann, K.H., Ber. Bunsenges. Phys. Chem. 83, 738 (1979).

32. Haynes, B.S. and Wagner, H.Gg., Progr. Energy Combust. Sci. 7, 229 (1981).

33. Takahashi, F. and Glassman, I., Combust. Sci. Tech. 37, 1 (1984).

34. Calcote, H.F. and Manos, D.M., Combust. Flame 49, 289 (1983).

35. Olson, D.B. and Pickens, J.C., Combust. Flame 57, 199 (1984).

36. Homann, K.H., Personal communication, August 1984.

37. Millikan, R.C., in Temperature; Its Measurement and Control in Science and Industry, Vol. 3, C.M. Herzfeld, Ed. (Reinhold Publishing Corp., New York, 1962) p. 497.

38. Hirschfelder, J.O., Curtiss, C.F., and Bird, R.B., Molecular Theory of Gases and Liquids, (Wiley, New York, 1954).

39. Benson, S.W., Thermochemical Kinetics, 2nd Ed. (Wiley, New York, 1976).

40. Harris, S.J. and Weiner, A.M., Combust. Sci. Tech. 31, 155 (1983).

41. Harris, S.J. and Weiner, A.M., Combust. Sci. Tech. 38, 75 (1984).

42. Harris, S.J. and Weiner, A.M., Ann. Rev. Phys. Chem. 36, 31 (1985).

43. Handbook of Physics and Chemistry, 61st Ed. (CRC Press, Boca Raton, 1980).

44. Krongauz, V.V. and Rabinovitch, B.S., Chem. Phys. 67, 201 (1982).

45. Barker, J.R. and Golden, R.E., J. Phys. Chem. 88, 1012 (1984).

46. Brown, T.C., Taylor, J.A., King, K.D., and Gilbert, R.G., J. Phys. Chem. 87, 5214 (1983).

47. Rossi, M.J., Pladziewicz, J.R., and Barker, J.R., J. Chem. Phys. 78, 6695 (1983).

48. Heymann, M., Hippler, H., and Troe, J., J. Chem. Phys. 80, 1853 (1984).

49. Kelley, D.F., Kasai, T., and Rabinovitch, B.S., J. Phys. Chem. 85, 1100 (1981).

50. Homann, K.H. and Stroefer, E., in Soot in Combustion Systems and Its Toxic Properties (J. Lahaye and G. Prado, Eds.), Plenum, New York, 1983, p. 217.

51. Stein, S.E., Combust. Flame 51, 357 (1983).

52. Olson, D.B. and Calcote, H.F., in Particulate Carbon: Formation During Combustion, D.C. Siegla and G.W. Smith, Eds. (Plenum Press, New York, 1981) p. 177.

53. Bonne, U., Homann, K.H., and Wagner, H. Gg., Tenth Symposium (International) on Combustion, (The Combustion Institute, Pittsburgh, 1965) p. 503.

54. Warnatz, J., Bockhorn, H., Moser, A., and Wenz, H.W., Nineteenth Symposium (International) on Combustion, (The Combustion Institute, Pittsburgh, 1982) p. 197.

55. Bittner, J.D. and Howard, J.B., Nineteenth Symposium (International) on Combustion, (The Combustion Institute, Pittsburgh, 1982) p. 211.

56. Anicich, V.G., Blake, G.A., Kim, J.K., McEwan, J.M., and Huntress, W.T., Jr., J. Phys. Chem. 88, 4608 (1984).

57. Eyler, J.R., in The Chemistry of Combustion Processes, T.M. Sloane, Ed., ACS Symposium Series 249, (American Chemical Society, Washington, DC, 1984), p. 49.

58. Laurendeau, N. M., Personal communication, 1986.

59. Homann, K.H. and Wagner, H.Gg., Eleventh Symposium (International) on Combustion, (The Combustion Institute, Pittsburgh, 1967), p. 371.

60. Calcote, H.F., in Ion-Molecule Reactions, J.L. Franklin, Ed., (Plenum Press, New York, 1972) p. 673.

61. Meot-Ner, M. Gas Phase Ion Chemistry, Vol. 1, M.T. Bowers, Ed., (Academic Press, New York, 1979), Ch. 6.

62. Patrick, R. and Golden, D.M., J. Chem. Phys. 82, 75 (1985).

63. Jennings, K.R., Headley, J.V., and Mason, R.S., Int. J. Mass Spectr. Ion Proc. 45, 315 (1982).

64. Smyth, K.C., Lias, S.G., and Ausloos, P., Combust. Sci. Tech. 28, 147 (1982).

65. Eyler, J.R., Ozlark, F., Baykut, and Moini, M., "Reactions of $C_3H_3^+$ with Acetylene and Diacetylene in the Gas Phase," to be submitted to J. Phys. Chem.

66. Calcote, H.F., Dynamics of Conducting Gases, Proceedings of the Third Biennial Gas-Dynamics Symposium, (Northwestern Univ. Press, Evanston, 1960), p. 36.

67. McDaniel, E.W. Collision Phenomena in Ionized Gases, (John Wiley, New York, 1964).

68. Olson, D.B. and Calcote, H.F., Eighteenth Symposium (International) on Combustion (The Combustion Institute, Pittsburgh, 1981) p. 453.

69. Clements, R.M. and Smy, P.R., J. Appl. Phys. 40, 4553 (1969).

70. Calcote, H.F., Ninth Symposium (International) on Combustion (The Combustion Institute, Pittsburgh, 1963) p. 622.

71. Homann, K.H., Ber. Bunsenges. Phys. Chem. 87, 1073 (1983).

TABLE 1
Suggested Structures of Some of the Observed Ions.

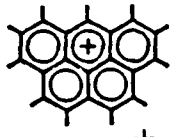

$C_{19}H_{11}^+$
239

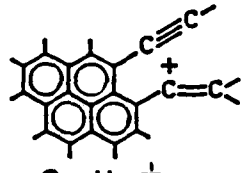

$C_{20}H_{11}^+$
251

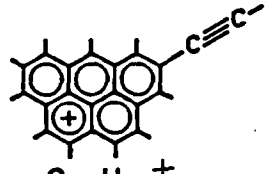

$C_{21}H_{11}^+$
263

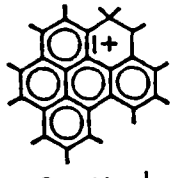

$C_{22}H_{13}^+$
277

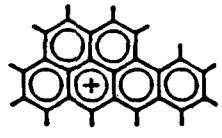

$C_{23}H_{13}^+$
289

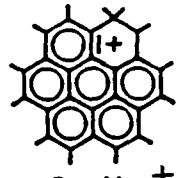

$C_{24}H_{13}^+$
301

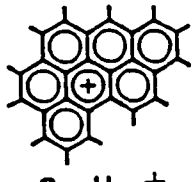

$C_{25}H_{13}^+$
313

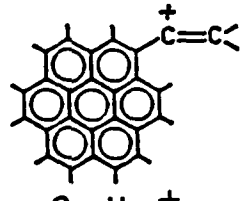

$C_{26}H_{13}^+$
325

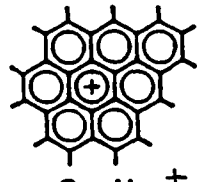

$C_{27}H_{13}^+$
337

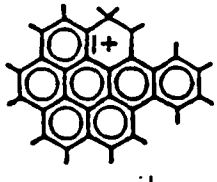

$C_{28}H_{15}^+$
351

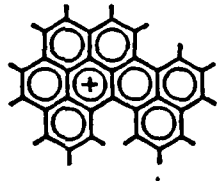

$C_{29}H_{15}^+$
363

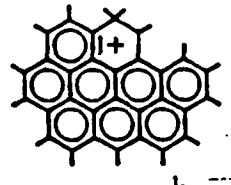

$C_{30}H_{15}^+$
375

TABLE I (continued)

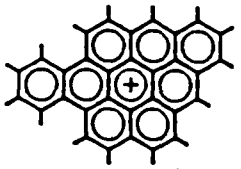

$C_{31}H_{15}^+$
387

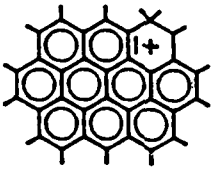

$C_{32}H_{15}^+$
399

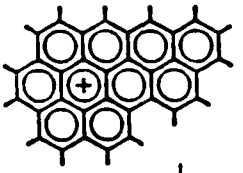

$C_{33}H_{15}^+$
411

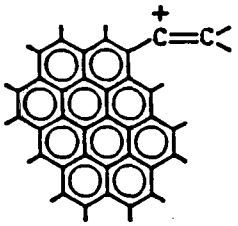

$C_{34}H_{15}^+$
423

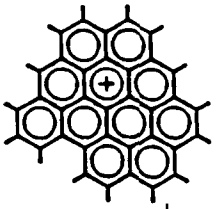

$C_{35}H_{15}^+$
435

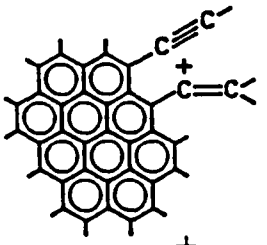

$C_{36}H_{15}^+$
447

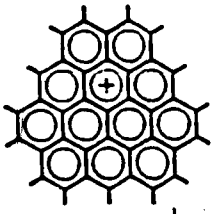

$C_{37}H_{15}^+$
459

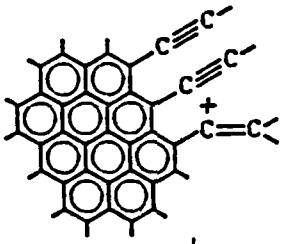

$C_{38}H_{15}^+$
471

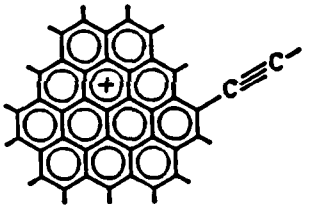

$C_{39}H_{15}^+$
483

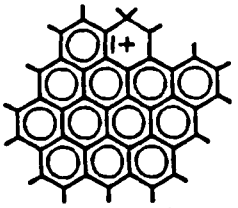

$C_{40}H_{17}^+$
497

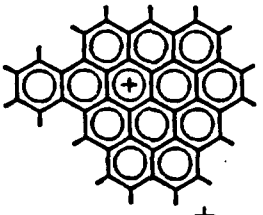

$C_{41}H_{17}^+$
509

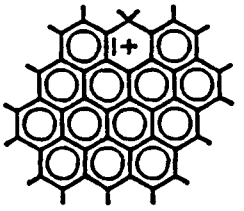

$C_{42}H_{17}^+$
521

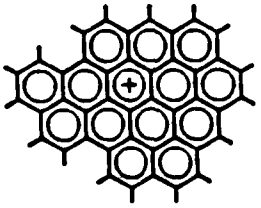

$C_{43}H_{17}^+$
533

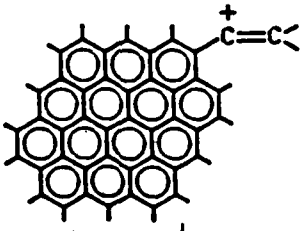

$C_{44}H_{17}^+$
545

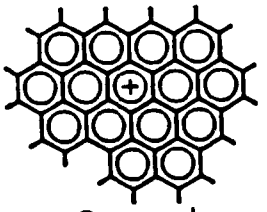

$C_{45}H_{17}^+$
557

TABLE II
Occurrence of Carbon and Hydrogen Atoms in Flame Ions.

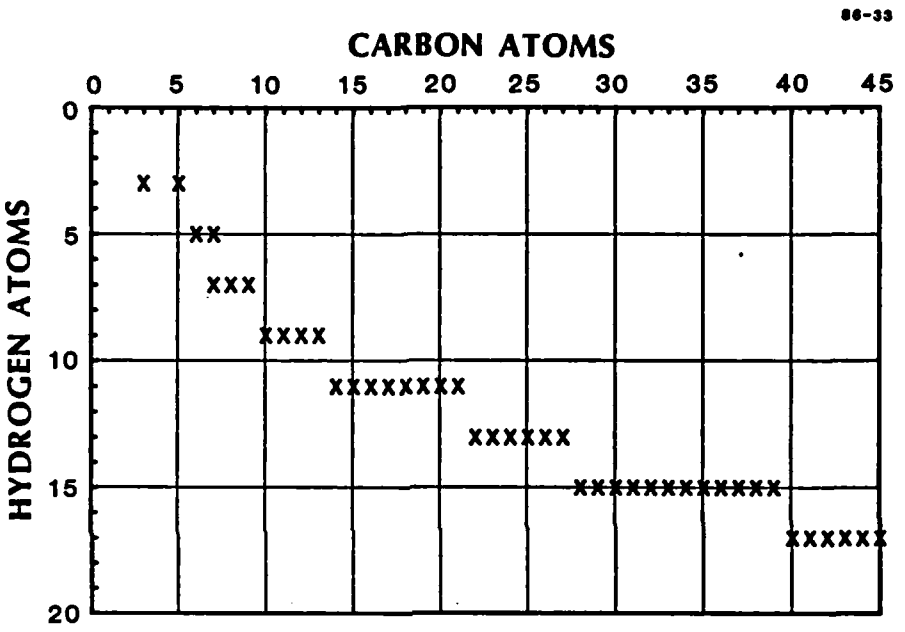

TABLE III

Rate Constants for Reaction of Neutrals with Ions to Produce Larger Ions.

Reactants		k(10^{-10} cm^3 s^{-1})		
Neutral	Ion[b,c]	From Characteristic Times[d]	Langevin, Estimated[a]	Experimentally Observed
C_2H_2	$C_3H_3^+$	0.0007	11	10 ,12[e,f,i]
C_2H_2	$C_{14}H_{11}^+$	0.0007	8	---
C_2H_2	$C_{45}H_{17}^+$	0.0007	9	---
C_4H_2	$C_3H_3^+$	0.02	7	10[e]
C_4H_2	$C_{14}H_{11}^+$	0.02	7	---
C_4H_2	$C_4H_3^+$	0.02	12	7.4[e]
C_3H_4(allene)	$C_3H_4^+$	0.4	8	11[e]
C_4H_4	$C_4H_3^+$	0.9	12	11[e]
C_6H_6	$C_3H_3^+$	3	16	14,[e] 15[f]
$C_{12}H_8$	$C_3H_3^+$	300	19[h]	6[f,h]
$C_{10}H_8$	$C_3H_3^+$	400	17	7[f]
$C_{14}H_8$	$C_3H_3^+$	1000	19[h]	6[f,h]

[a] Estimated with Langevin's theory using polarizabilities calculated from refractive indices and Lorentz-Lorenz equation.

[b] Ion in "estimated" and "observed" reactions.

[c] Linear $C_3H_3^+$ assumed (see text).

[d] Independent of ion (see text).

[e] Smyth et al.[54].

[f] Eyler.[57]

[g] Anicich et al.[56]

[h] For 1-methylnaphthalene, $C_{11}H_{10}$.

[i] Eyler and associates[55] report a much lower rate coefficient for this reaction.

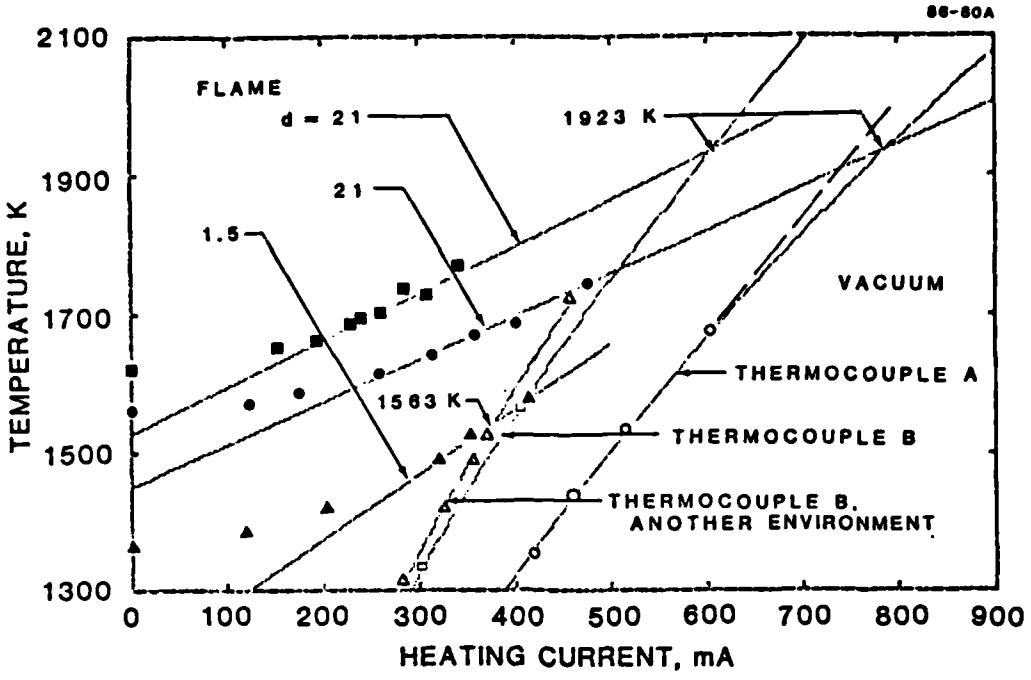

FIGURE 1 THERMOCOUPLE HEATING CURVES IN VACUUM (OPEN SYMBOLS) AND IN Ø = 2.25 FLAMES (CLOSED SYMBOLS)

Distances from the burner are given in mm. The intersections of matched solid curves (see text) give the indicated experimental flame temperatures. Dashed curve - linear extrapolation of thermocouple A vacuum data (see text).

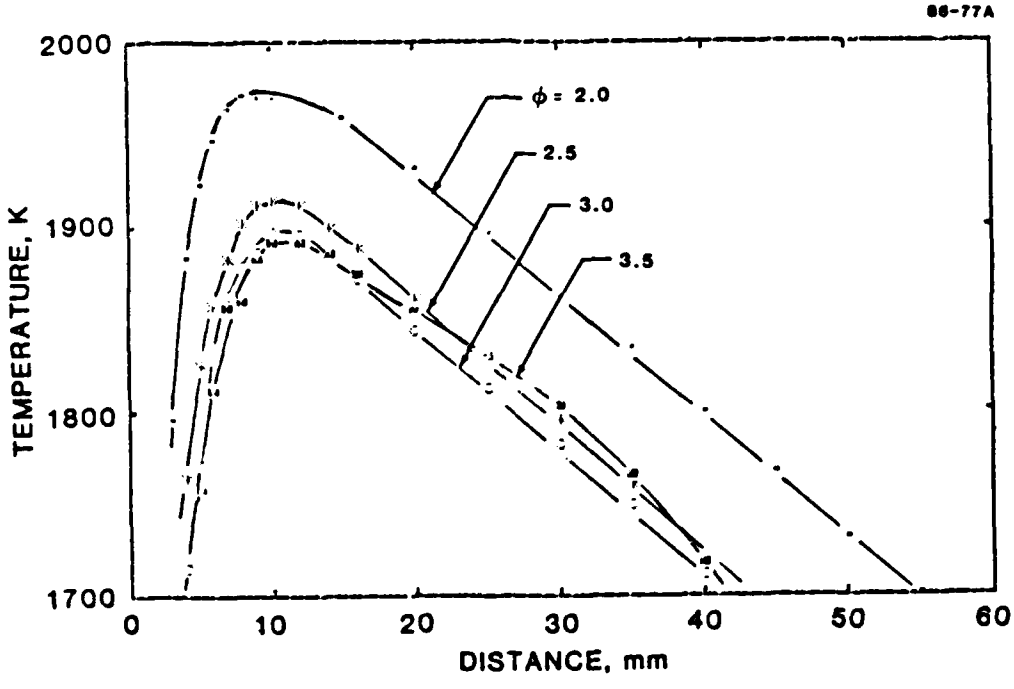

FIGURE 2 EXPERIMENTAL TEMPERATURE PROFILES FOR ACETYLENE-OXYGEN FLAMES FOR DIFFERENT EQUIVALENCE RATIOS

Stainless steel burner, low pressure flames (see text).

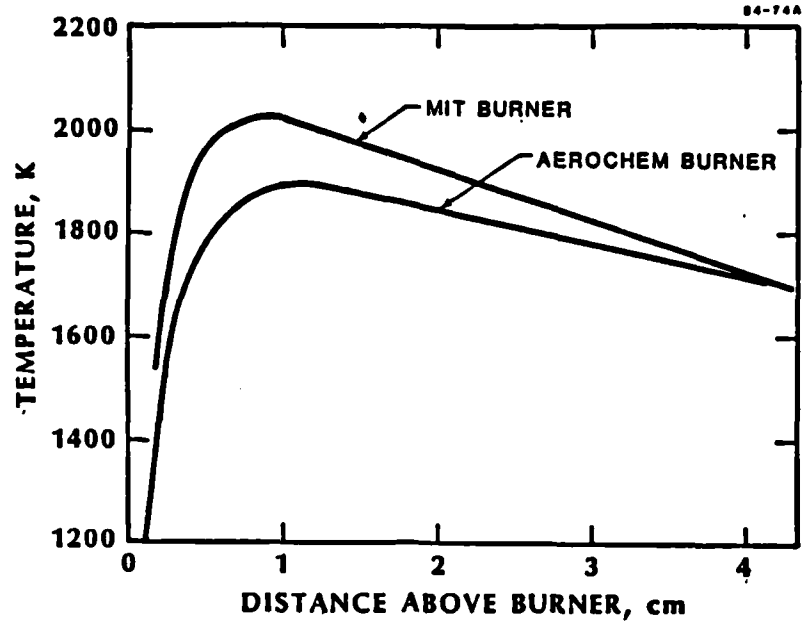

FIGURE 3 COMPARISON OF TEMPERATURE PROFILES IN THE MIT DESIGN COPPER BURNER AND THE AEROCHEM STAINLESS STEEL MULTITUBE BURNER

Ø = 3.0 flames (see text).

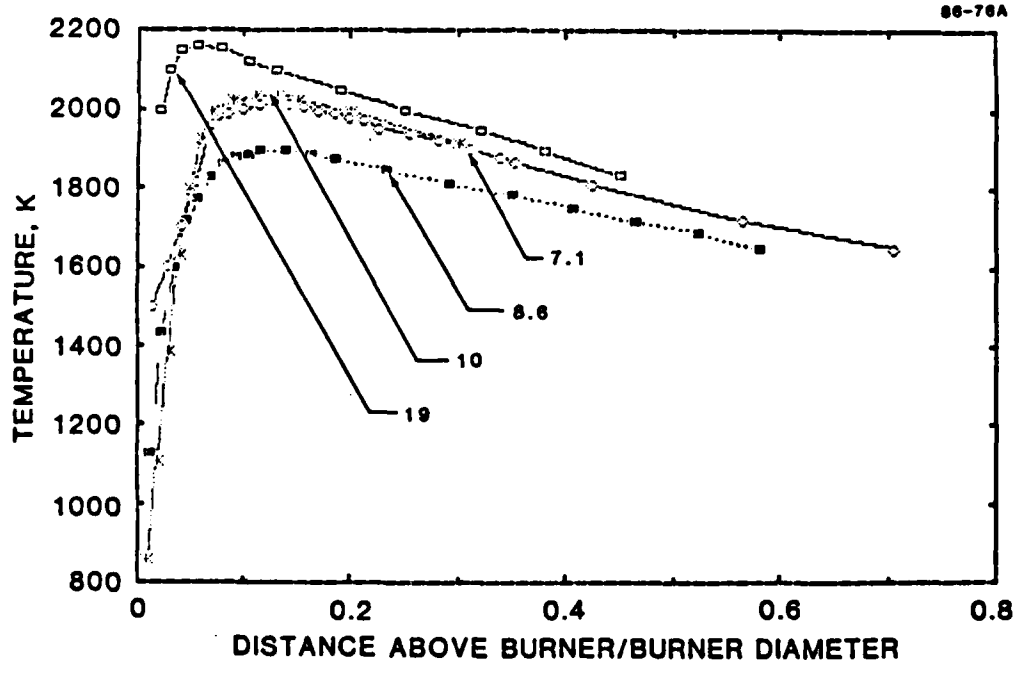

FIGURE 4 TEMPERATURE PROFILES AS FUNCTION OF DISTANCE ABOVE BURNER NORMALIZED BY BURNER DIAMETER

□ - Ref. 21, Ø = 3.5; * - Ref. 9 with diameter from Ref. 8 assumed;
○ - MIT design copper burner; ■ - AeroChem stainless steel burner.
All acetylene-oxygen flames (p = 2.7 kPa, u = 50 cm/s). Ø = 3.0 unless noted otherwise. Diameters indicated in cm.

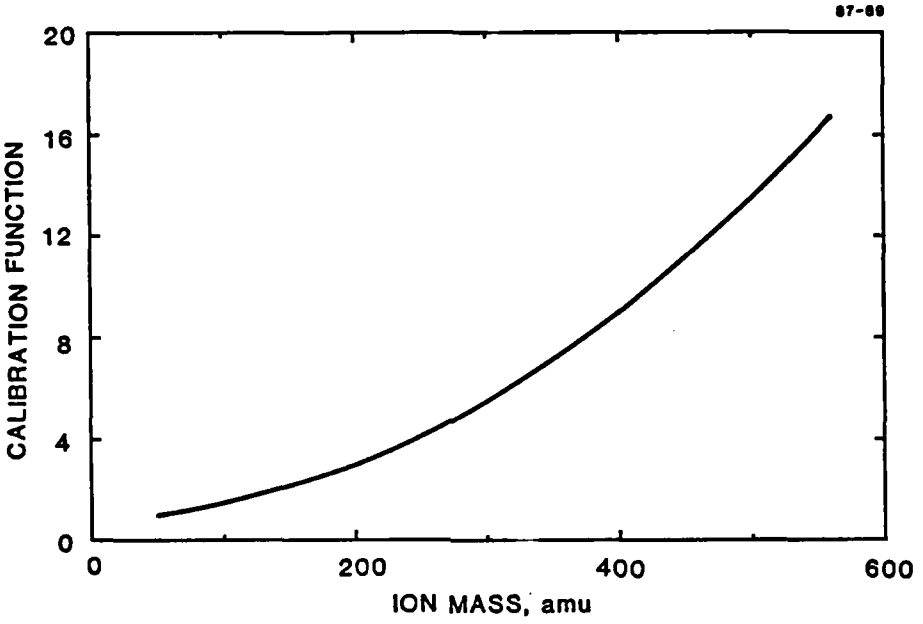

FIGURE 5 MASS CALIBRATION FUNCTION

Multiplicative function derived to correct mass spectrometer ion currents for relative mass discrimination effects.

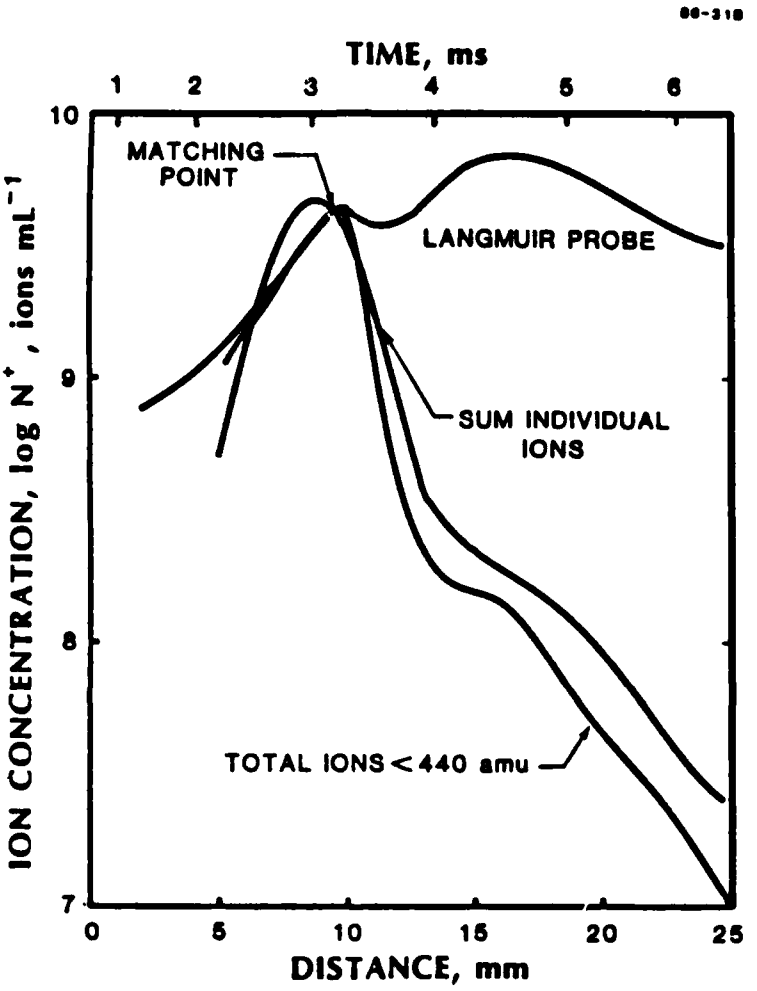

FIGURE 6 COMPARISON OF TOTAL ION CONCENTRATION PROFILE FROM LANGMUIR PROBE MEASUREMENTS[23] WITH PRESENT MASS SPECTROMETER MEASUREMENTS

Adjusted mass spectrometer current profiles (see text) have been normalized by a constant factor to make the sum of individual ion currents agree with Langmuir probe results at 10 mm.

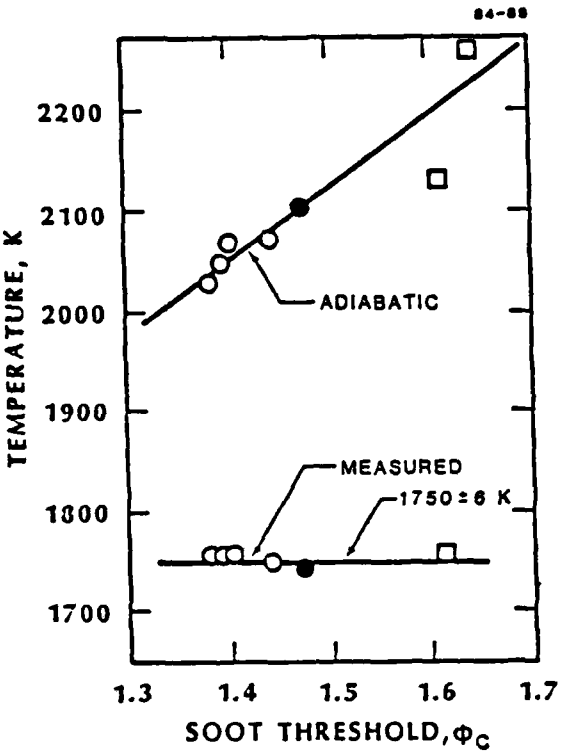

FIGURE 7 COMPARISON OF ADIABATIC AND MEASURED TEMPERATURES AS A FUNCTION OF SOOT THRESHOLD, ϕ_c, FOR ATMOSPHERIC TOLUENE/O_2/N_2 FLAMES

○ - $O_2/(O_2 + N_2)$ (0.21; ● - Fuel-Air Mixtures
□ - $O_2/(O_2 + N_2)$) 0.21.

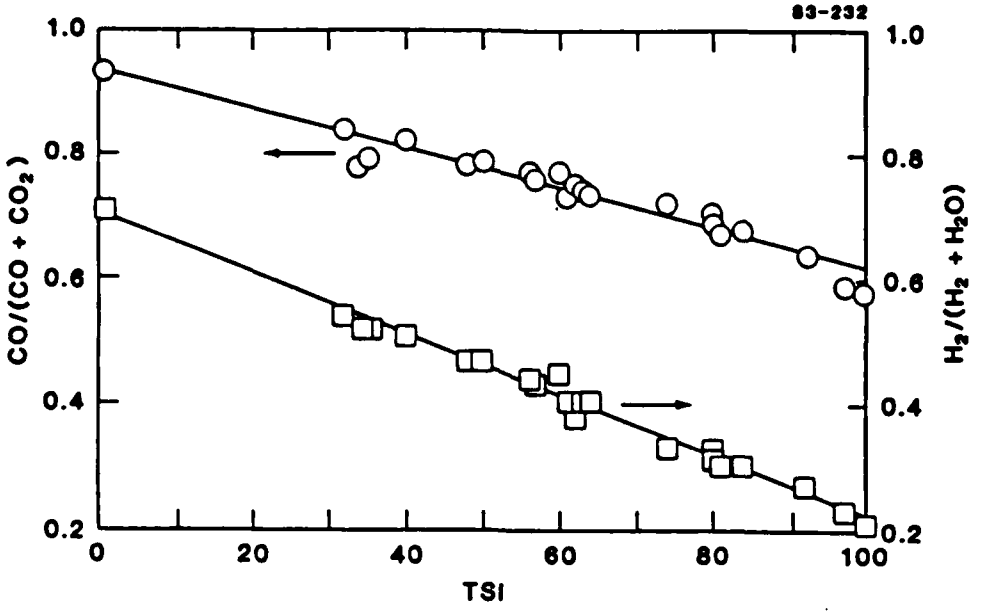

FIGURE 8 EQUILIBRIUM COMPOSITIONS CALCULATED AT THE MEASURED SOOT THRESHOLD FOR A SERIES OF FUELS

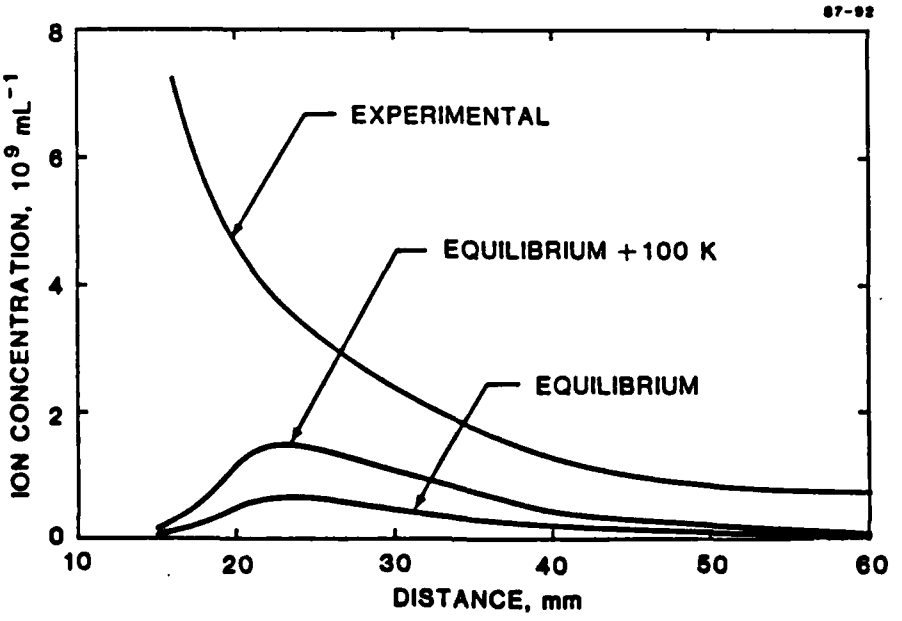

FIGURE 9 COMPARISON OF EQUILIBRIUM CALCULATIONS OF CHARGED SOOT (POSITIVE ION) CONCENTRATIONS WITH MEASURED CONCENTRATIONS

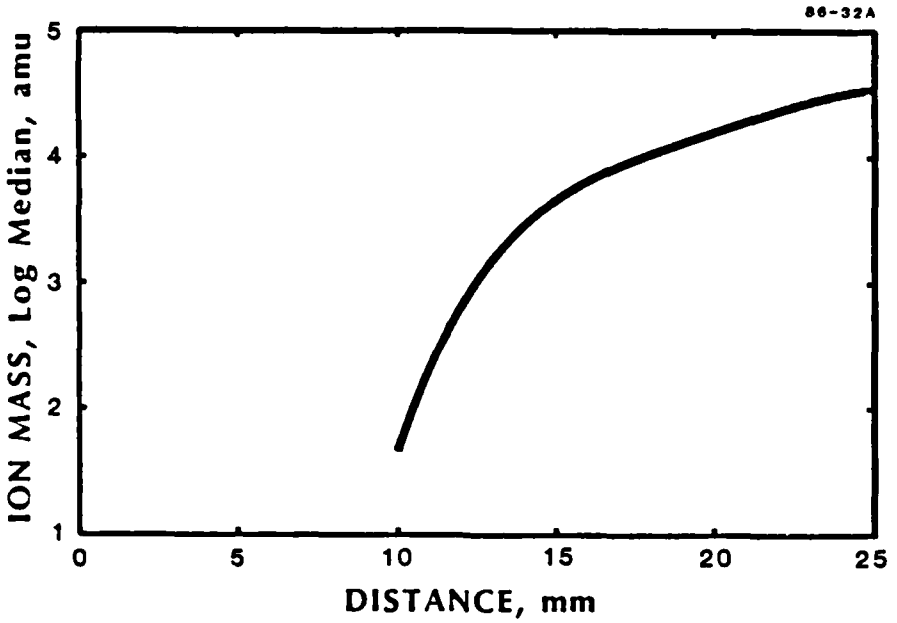

FIGURE 10 INCREASE IN ION MASS WITH DISTANCE ABOVE BURNER DEDUCED FROM HOMANN AND STROEFER'S MEASUREMENTS[23,50]

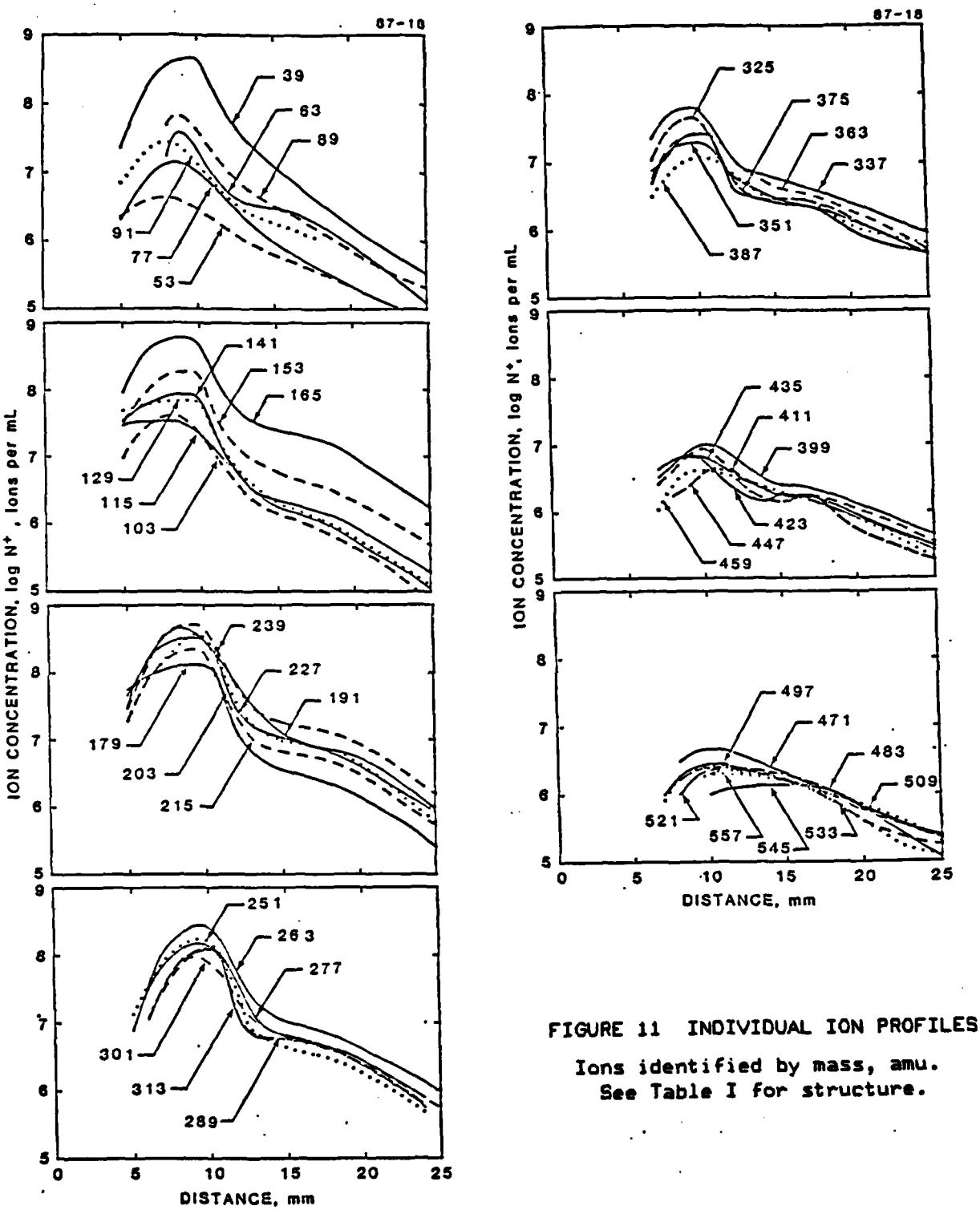

FIGURE 11 INDIVIDUAL ION PROFILES

Ions identified by mass, amu.
See Table I for structure.

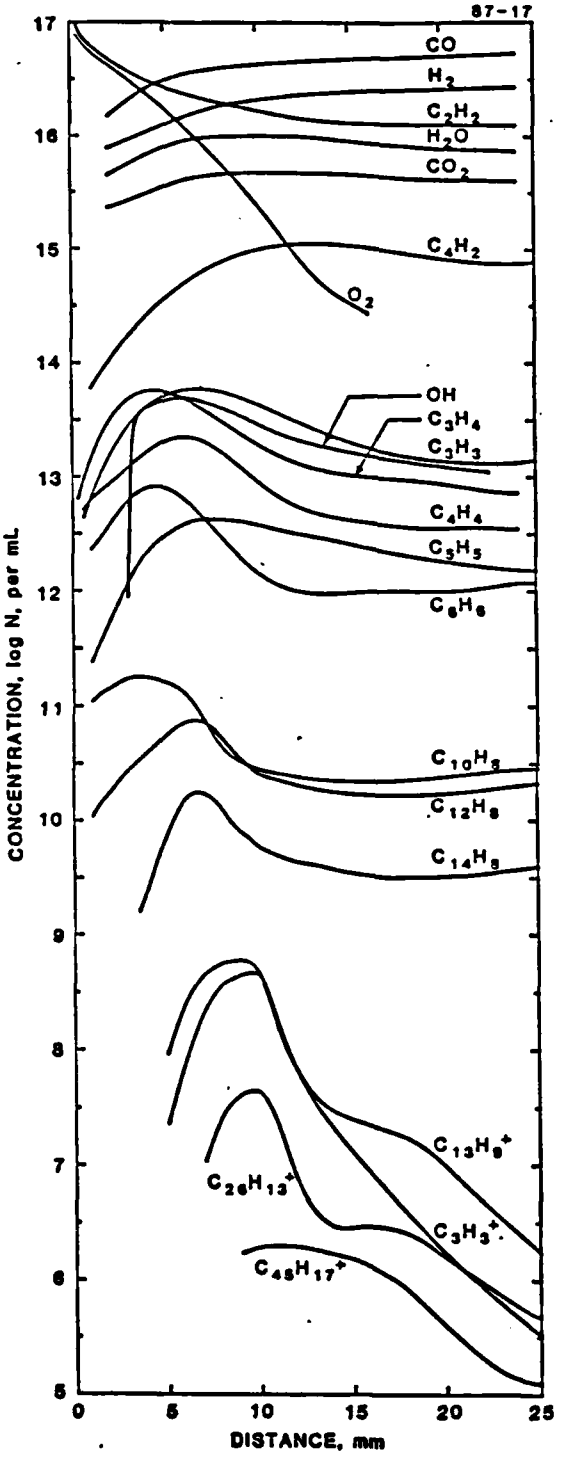

FIGURE 12 CONCENTRATION PROFILES OF SELECTED NEUTRAL AND IONIC SPECIES

OH profiles from Ref. 58. Neutral profiles were calculated from published mole fraction profiles. C_2H_2 and O_2 profiles are from Fig. 11, Ref. 5 (multiplied by 2 due to an apparent error in the figure) and are indistinguishable from those of Delfau and Vovelle (DV) in Ref. 9. Other profiles from Bittner and Howard (BH) in Ref. 5 include $C_{10}H_8$, $C_{12}H_8$, and $C_{14}H_8$. Profiles of CO, H_2, CO_2, H_2O, C_3H_3, C_3H_4, and C_5H_5 are from DV. Profiles for C_4H_2 and C_4H_4, reported by both BH and DV, are, respectively similar in shape and magnitude (< factor of 2 difference) and were averaged for presentation here. The corresponding profiles for C_6H_6 were also averaged although they were significantly different. From BH, the C_6H_6 maximum occurs at 7 mm while DV show the maximum at 4 mm. Also, DV found lower mole fractions by as much as a factor of 10. Selected ion profiles are from this work.

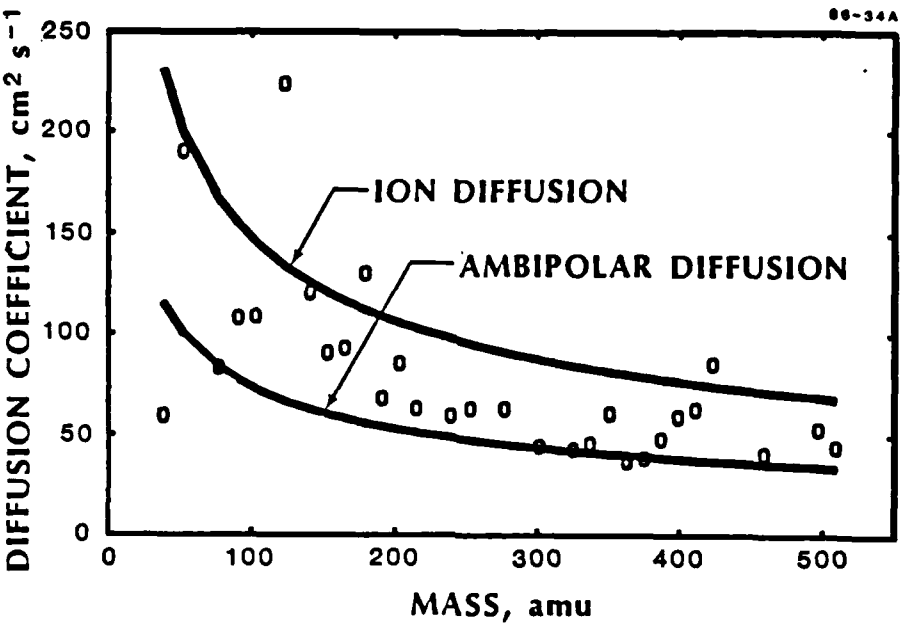

FIGURE 13 COMPARISON OF MEASURED (POINTS) WITH CALCULATED (LINES) DIFFUSION COEFFICIENTS

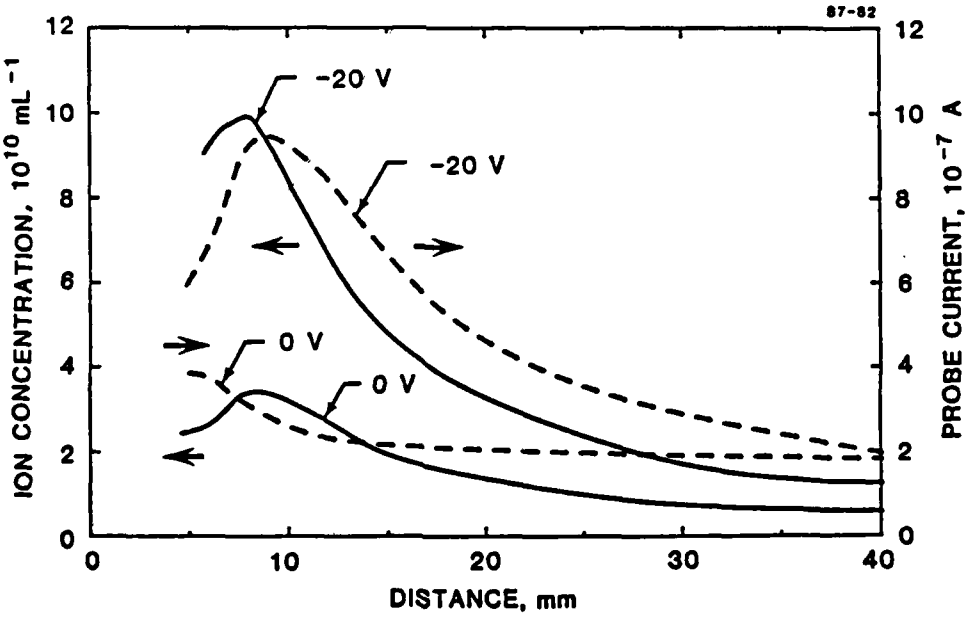

FIGURE 14 LANGMUIR PROBE CURRENT AND ION CONCENTRATION PROFILES

Experimental currents at plasma potential (0 V) and at -20 V extracted from I/V curves at each distance in Ø = 1.8 flame. The calculated ion concentrations were based on theory appropriate to the collection voltage. See text.

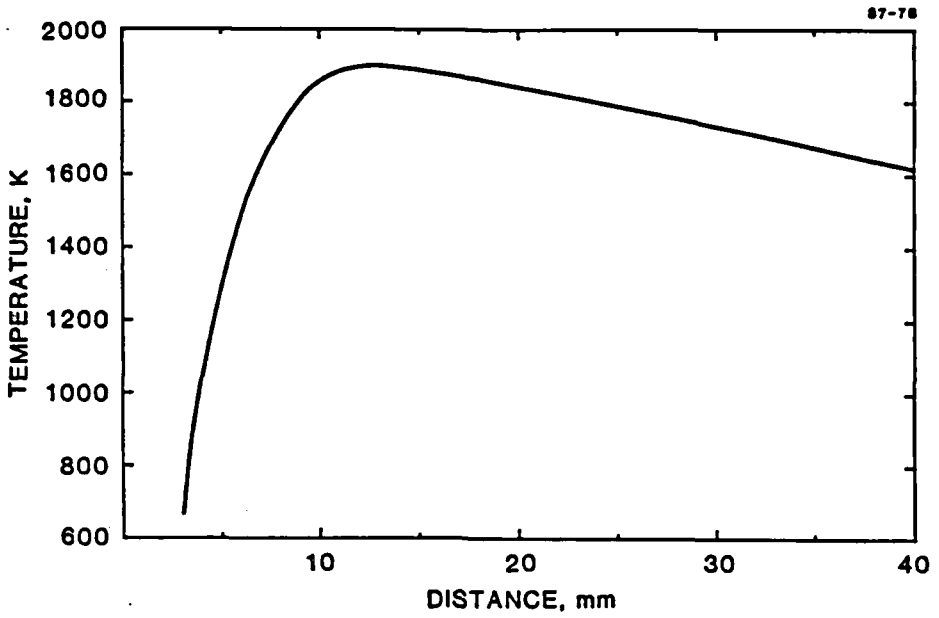

FIGURE 15 TEMPERATURE PROFILE IN Ø = 1.8 FLAME

Experimental temperature profile for Ø = 1.8 benzene/oxygen/30% argon flame corrected for effect of sampling cone, from Ref.5.

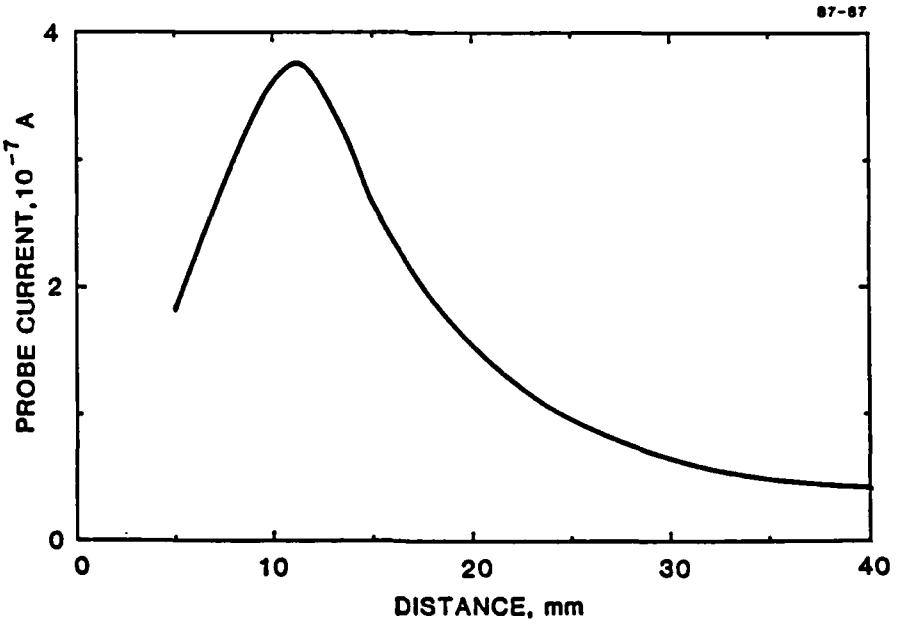

FIGURE 16 LANGMUIR PROBE CURRENT PROFILE

Probe currents at -20 V from I/V curves in Ø = 2.0 flame, see text.

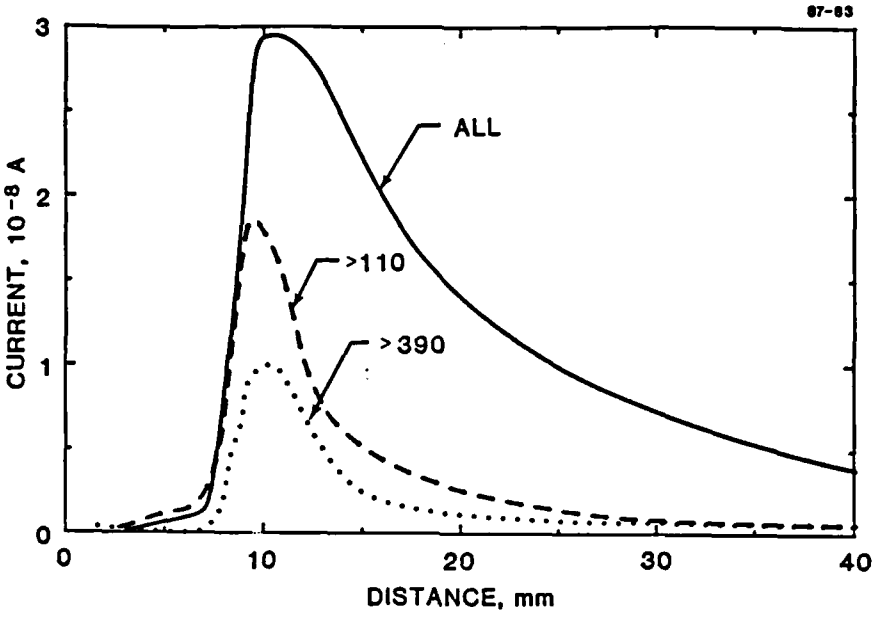

FIGURE 17 HIGH PASS FILTER MASS SPECTROMETER PROFILES

Total mass spectrometer current profiles in three high pass filter modes: passing ALL ions, ions > 110 amu, and ions > 390 amu. Ø = 1.8 flame. Solid curve shifted 0.5 mm towards the burner.

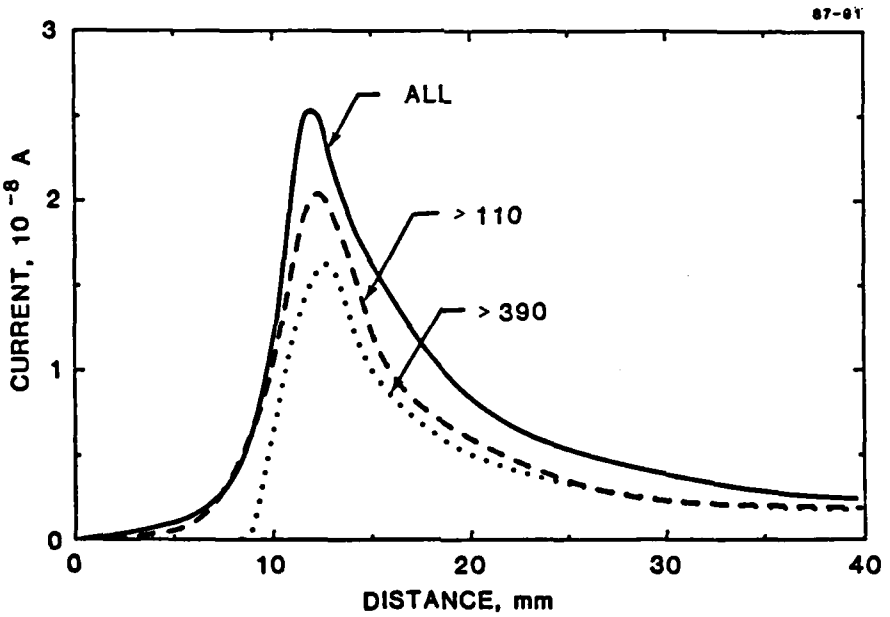

FIGURE 18 HIGH PASS FILTER MASS SPECTROMETER PROFILES

Total mass spectrometer current profiles in three high pass filter modes: collecting ALL ions, ions > 110 amu, and ions > 390 amu. Ø = 2.0. Each curve represents an average of three separately recorded profiles. The solid curve has been shifted 0.5 mm towards the burner.

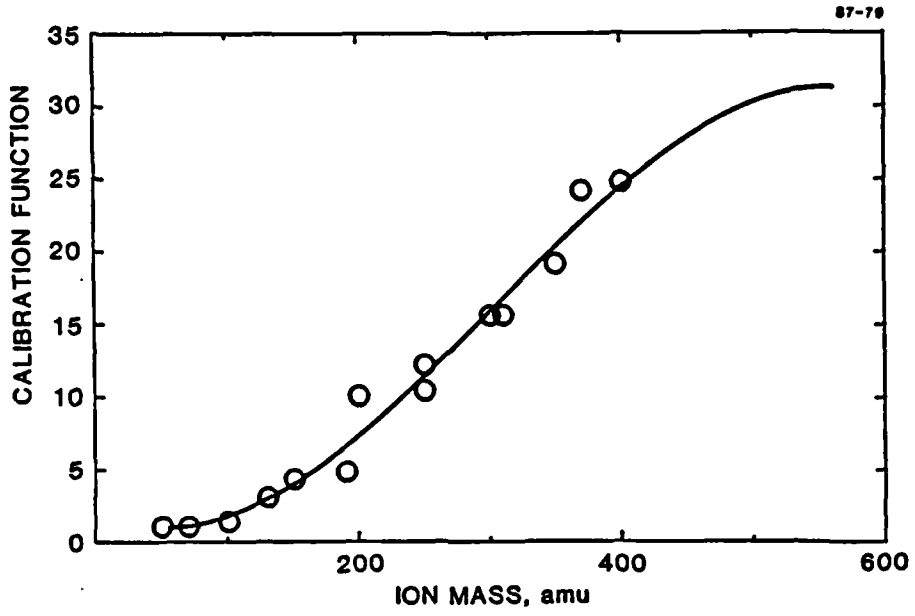

FIGURE 19 MASS SPECTROMETER SENSITIVITY CALIBRATION FUNCTION

Relative mass spectrometer sensitivity as deduced from ratio of currents collected in two modes of operation in Ø = 1.8 flame, see text. Symbols represent experimental current ratios over 50 amu or 60 amu mass ranges versus the mass range midpoint. The curve is a least-squares cubic polynomial fit to the symbols.

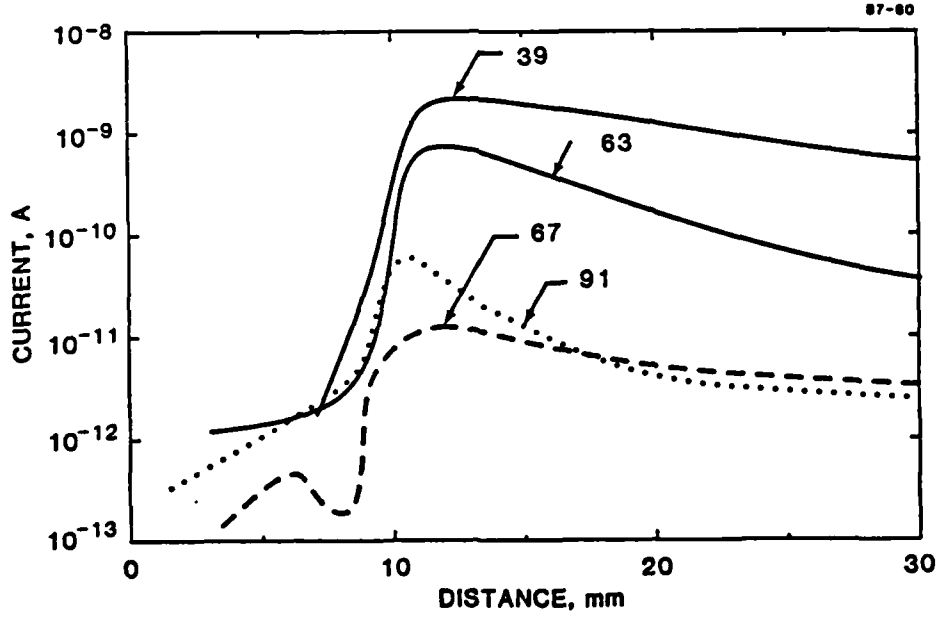

FIGURE 20 INDIVIDUAL ION PROFILES IN Ø = 1.8 FLAME

Selected mass spectrometer logarithmic current profiles for individual ions as indicated by mass in amu.

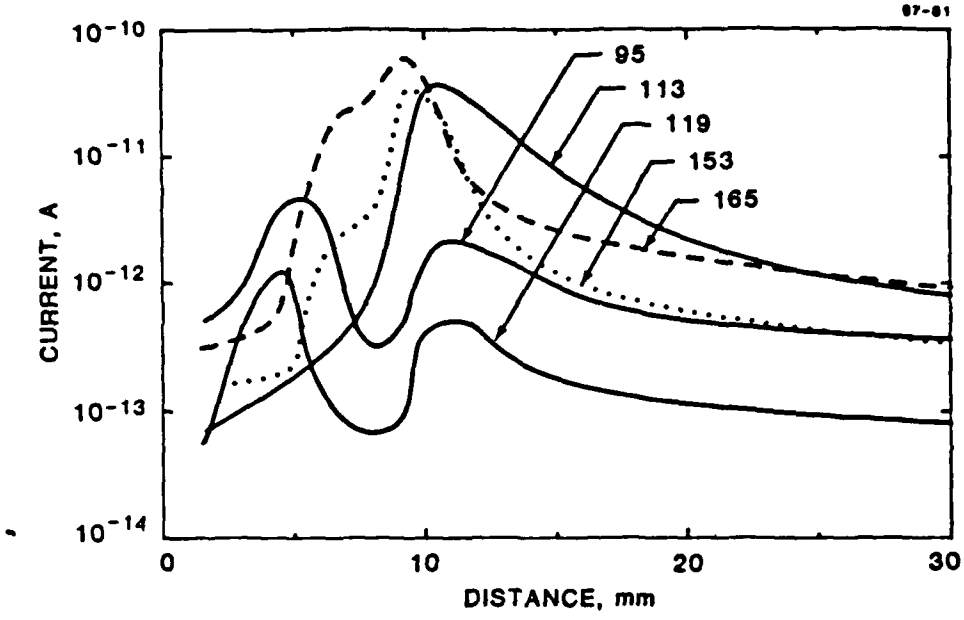

FIGURE 21 INDIVIDUAL ION PROFILES IN Ø = 1.8 FLAME

Selected mass spectrometer logarithmic current profiles for individual ions as indicated by mass in amu.

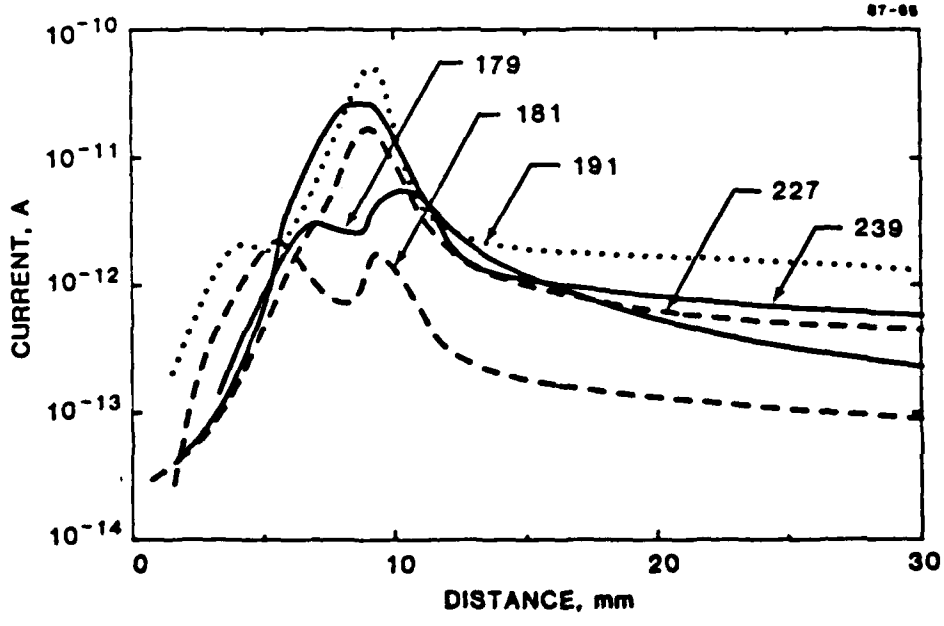

FIGURE 22 INDIVIDUAL ION PROFILES IN Ø = 1.8 FLAME

Selected mass spectrometer logarithmic current profiles for individual ions as indicated by mass in amu.

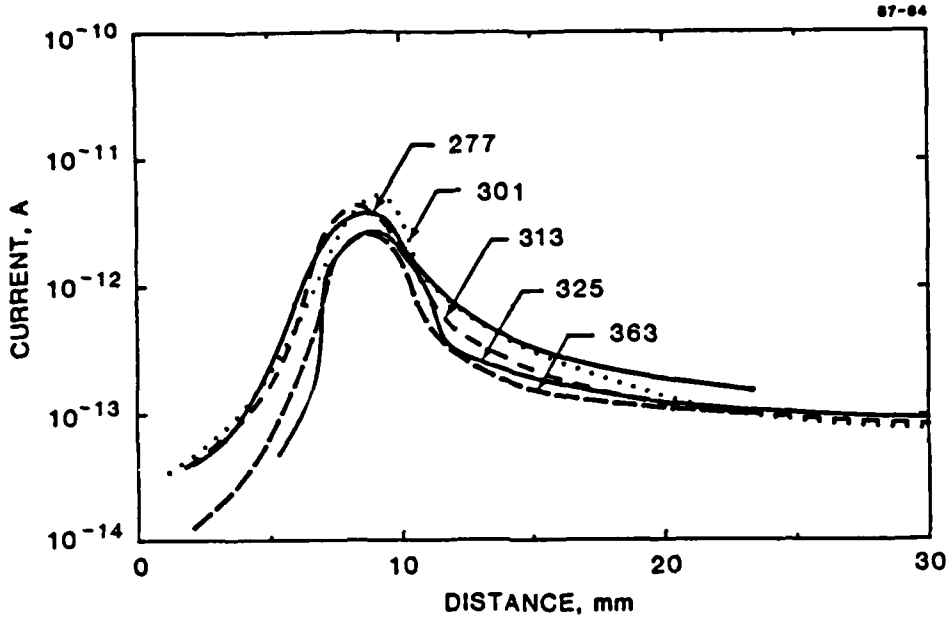

FIGURE 23 INDIVIDUAL ION PROFILES IN Ø = 1.8 FLAME

Selected mass spectrometer logarithmic current profiles for individual ions as indicated by mass in amu.

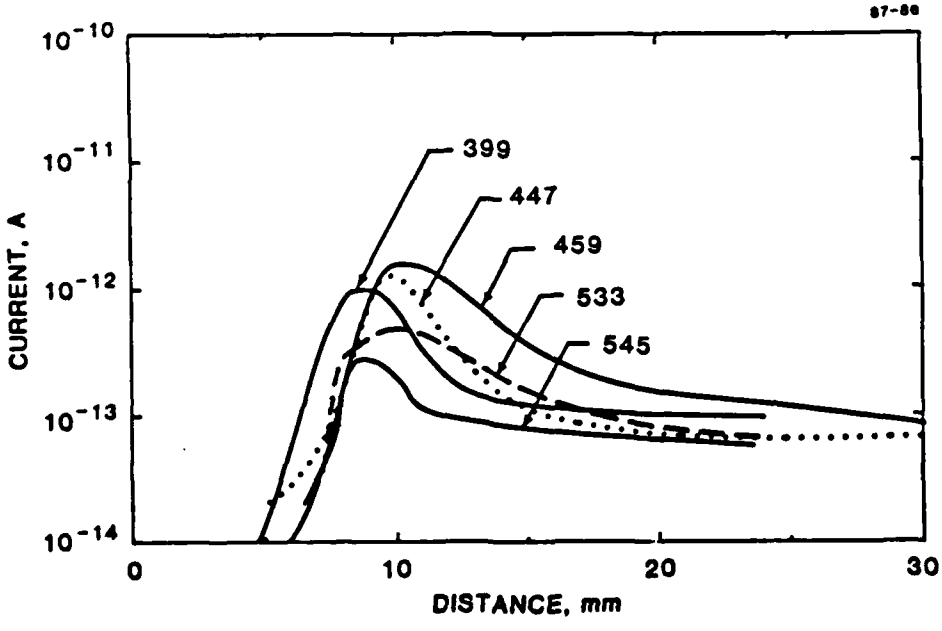

FIGURE 24 INDIVIDUAL ION PROFILES IN Ø = 1.8 FLAME

Selected mass spectrometer logarithmic current profiles for individual ions as indicated by mass in amu.

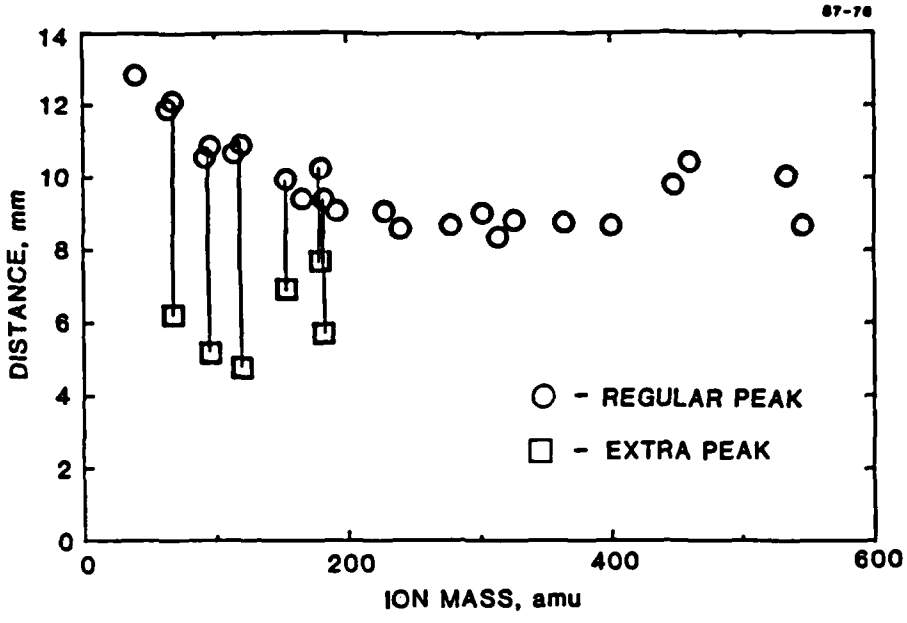

FIGURE 25 LOCATION OF CURRENT MAXIMA IN ION PROFILES

Distance above the burner where individual ion mass profiles maximize as a function of mass in $\emptyset = 1.8$ flame. Species profiles exhibiting two peaks are indicated as a vertical line joining the two peak locations.

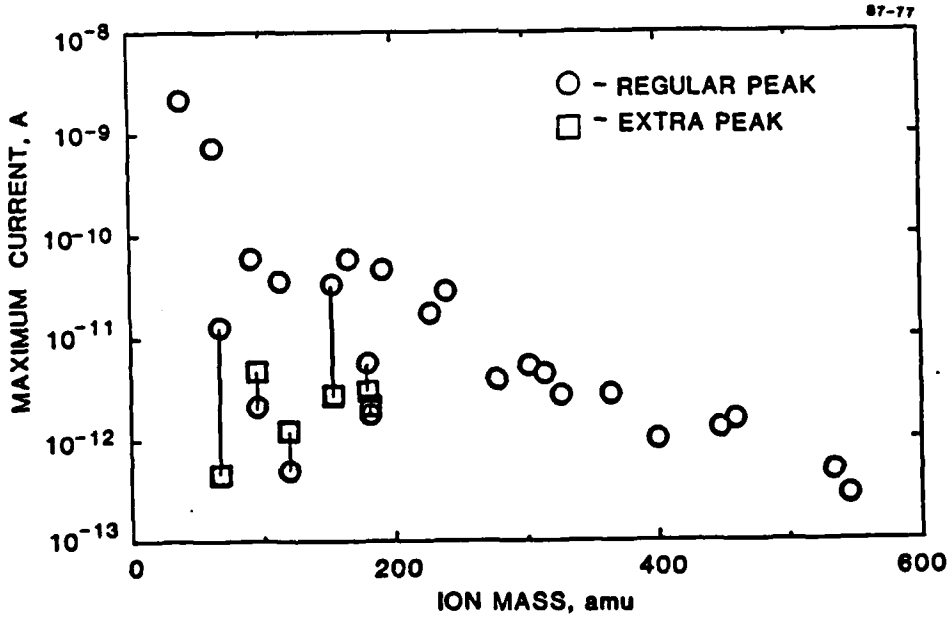

FIGURE 26 MAXIMUM CURRENTS IN ION PROFILES

Maximum mass spectrometer currents in ion profiles plotted as a function of the ion mass. These maxima correspond to the same ions in the same flame as in Fig. 25.

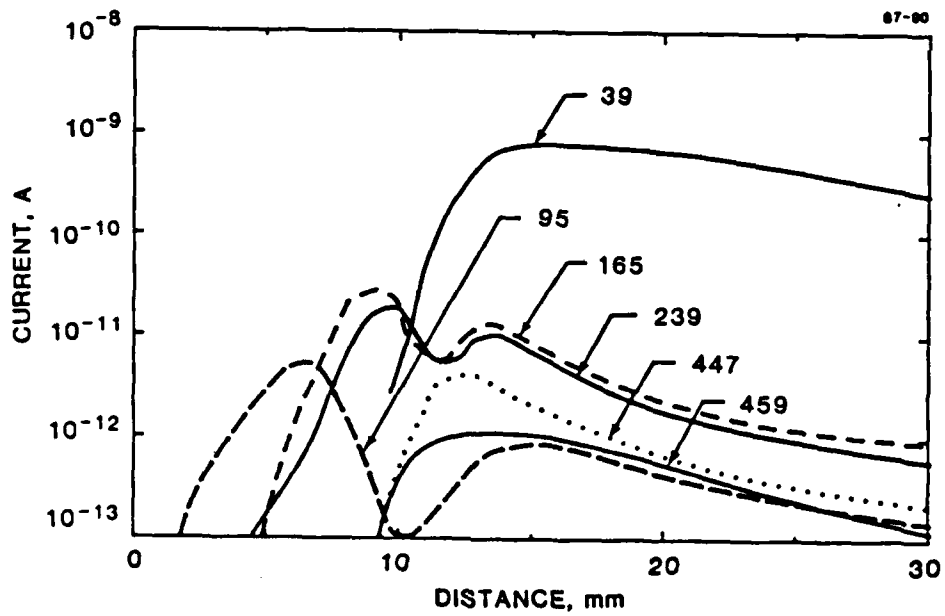

FIGURE 27 INDIVIDUAL ION PROFILES IN Ø = 2.0 FLAME

Selected mass spectrometer logarithmic current profiles for individual ions as indicated by mass in amu.

END

DATE

FILMED

DEC.

1987